NASA TN D-1874

NASA TN D-1874

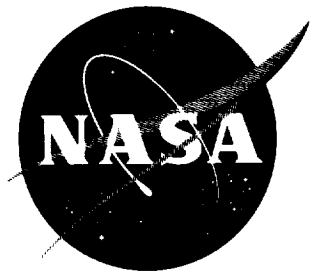

TECHNICAL NOTE

D-1874

DIRECTIONAL BEHAVIOR OF EMITTED AND REFLECTED RADIANT ENERGY FROM A SPECULAR, GRAY, ASYMMETRIC GROOVE

By John R. Howell and Morris Perlmutter

Lewis Research Center
Cleveland, Ohio

NATIONAL AERONAUTICS AND SPACE ADMINISTRATION

WASHINGTON

August 1963

NATIONAL AERONAUTICS AND SPACE ADMINISTRATION

TECHNICAL NOTE D-1874

DIRECTIONAL BEHAVIOR OF EMITTED AND REFLECTED RADIANT ENERGY FROM A SPECULAR, GRAY, ASYMMETRIC GROOVE

By John R. Howell and Morris Perlmutter

SUMMARY

19179

The directional emissivity and directional reflectivity of a specular, gray, isothermal groove are analyzed. A general method of analysis based on images of surfaces is given. The apparent directional emissivity, which is shown to be equal to the apparent directional absorptivity for any isothermal cavity, is presented as a function of groove parameters and the emissivity of the material. The apparent directional reflectivity is presented as a function of these parameters and the angle of incidence of the incident radiation. The results indicate that the directional radiant properties are strongly dependent on the shape of the local macroscopic surface structure, which is considered large relative to the wavelengths of the radiant energy. It is shown that the radiant energy interchange between surfaces can be directed and controlled by proper design of these surfaces.

INTRODUCTION

In most analyses dealing with radiant interchange between surfaces, the assumption is made that emission from surfaces is diffuse, that is, follows Lambert's cosine law. Reflection is assumed to occur in either a diffuse or a specular (mirrorlike) fashion. It has been stated in references 1 and 2 that these are only limiting cases for real surfaces, and the actual angular distribution of energy can vary widely from these simple cases. Reference 3 gives integral equations that can be used to calculate the radiant interchanges for surfaces with directional properties.

An important cause of the deviation of real surfaces from these limiting cases of specular and diffuse reflection and diffuse emission is the local macroscopic surface profile. This profile may cause large discrepancies in measured radiative properties of materials if the specimens used are not correctly prepared so that the surface irregularities are small compared to the wavelength of the radiation. The use of diffuse or specular surface properties in the calculation of radiant interchange can lead to gross deviations from the true case. The present work is an effort to investigate these effects.

By intentionally shaping the surface structure so that known directional

radiation characteristics are obtained, it is possible to influence the radiant heat exchange between surfaces. For example, a heat sink for radiant energy would be more efficient if it could have a high absorptivity in the direction of a heat source and a low emissivity in the direction of the cold environment. A poor heat sink could be obtained by interchanging these characteristics.

A heat-emitting surface could be made to emit strongly in the direction of a heat sink and weakly in other directions, and heat losses to the environment would thereby be reduced. If a reflecting surface could be designed to reflect strongly in any desired direction, energy could then be reflected to a specific location. A use of this type of reflecting surface is given in reference 4, where a Fresnel reflector, a disk with concentric mirrored grooves, was used to focus solar energy to a small area.

The configuration studied herein is a surface consisting of adjoining right-triangular grooves, as shown in figure 1. The surfaces are assumed to be gray, that is, with monochromatic wall absorptivity independent of wavelength and therefore with total emissivity equal to total absorptivity. The present analysis also applies at a given wavelength for the nongray case, and the complete solution would be obtained by summing the results at each wavelength over the spectrum of interest.

There is radiation (from an emitter) incident on the surface at a given angle. The reflections are assumed to take place specularly at the surface that is isothermal and that is assumed to emit diffusely. Assuming the surface emits diffusely and reflects specularly is not inconsistent with earlier arguments.

In reference 5, the net emission from a symmetric groove was calculated. The present analysis differs in that it uses an asymmetric configuration and examines the directional behavior of the emission, absorption, and reflection.

SYMBOLS

D	distance between parallel planes
$d^2F_{dA_1\text{-}dA_2}$	shape factor
f_n	fractional part of unattenuated beam that is reflected out of groove from image surface n
H	height of groove wall normal to base plane
I	length of oblique or normal wall of groove divided by H (eq. (8))
L	length of oblique wall
M,N	limits of summation (eq. (21))
n	image index

$n'-1$	defines image of surface from which part of incident beam first is reflected out of groove
Q	energy per unit time
q	energy per unit area per unit time
T	temperature of surface
X	distance along oblique side of groove divided by H
Y	distance along normal side of groove divided by H
Z	coordinate axis perpendicular to X and Y
α	absorptivity
β	angle between normal to X-surface and emitted beam
β'	angle between normal to X-surface and incident beam
$\Delta E, \Delta R$	width of emitter or receiver, respectively
ϵ	emissivity
ϵ_η	directional emissivity; ratio of energy emitted by groove and incident on element in direction η divided by energy emitted by flat, black surface to same element
η	angle between normal to base plane and beam to receiver, $\theta + \beta - \pi/2$
η'	angle between normal to base plane and incident beam, $\theta + \beta' - \pi/2$
$\eta_{X,n}, \eta_{Y,n}$	direction of reflection of part of beam incident on X- or Y-surface, respectively
θ	open angle between walls of groove
λ_n	inner boundary of beam reflected off image of surface n and emerging from groove
Ξ	aspect ratio; ratio of width of plane to distance apart for parallel plane geometry (fig. 9)
ξ	distance along base plane divided by distance between plates
ρ	reflectivity

$\rho_{\eta',\eta}$	directional reflectivity for incident beam η' reflected in direction η
σ	Stefan-Boltzmann constant
ψ	angle between normal to Y-surface and emitted beam
ψ'	angle between normal to Y-surface and incident beam

Subscripts:

a	absorbed
b	black, $\epsilon = 1$
ΔE-X	from emitter to surface X
ΔE-Y	from emitter to surface Y
E	emitter surface
e	emitted
l	lower limit of emitted beam (figs. 2 and 3)
l'	lower limit of incident beam
max	maximum
n=0,1,2. . .	surface image number (figs. 2 and 3)
u	upper limit of emitted beam
u'	upper limit of incident beam
w	wall of groove
X-ΔR	from surface X of area $H^2X\ dZ$ to receiver
Y-ΔR	from surface Y of area $H^2Y\ dZ$ to receiver
Ξ	absorbing surface
ξ	position along base plane

ANALYSIS

The surface analyzed is shown in figure 1 and consists of grooves of infinite length. The short side of the groove is normal to the base plane and of height H. There is some angle θ between the walls of the groove. (The

diagonal side is of length $L = H/\cos\theta$.) The surface of the groove is considered to be at temperature T_w with a gray emissivity ϵ_w. At the surface, the emitted energy is assumed to be diffuse, while the reflected energy is assumed to be reflected specularly. The problem can be divided into two parts: (1) The directional emission of energy from the grooves, and (2) the directional reflection and absorption of energy by the grooves for a given incident beam direction. First, the directional emission is calculated.

DIRECTIONAL EMISSION

The rate of energy being emitted per unit area from the surface at temperature T_w is q_w. A receiver of small width ΔR, infinite in the Z-direction, is located so that it will intercept all the radiation leaving the groove by emission within the angular increment that it subtends. The distance from the receiver to the groove is considered to be large compared with H and L. The energy incident from the environment is neglected.

This problem can be divided into three cases dependent on whether: (1) Part of side X is visible directly to the receiver, but none of side Y, (2) part of side Y is visible directly but none of X, and (3) both X and Y are directly visible. These cases are illustrated in figures 2 and 3 by the broken lines.

Side X Directly Visible to Receiver

The power reaching the receiver directly from an infinitesimal element of area $H^2\,dX\,dZ$ on the part of side X visible to the receiver is $q_w H^2\,dX\,dZ\,d^2F_{dX-\Delta R}$. This same amount of power will be incident on the receiver from every element along Z for X fixed. The relation for the shape factor $d^2F_{dX-\Delta R}$ is obtained from reference 6 (eq. 31-58) and is

$$d^2F_{dX-\Delta R} = \frac{\cos\beta}{2}\,\Delta\beta \tag{1}$$

The angle β is shown in figures 1 and 2. Since q_w and β are assumed to be constant over the groove surface, the radiant power reaching the receiver directly can be written as

$$Q_{O,X-\Delta R} = q_w \frac{\cos\beta}{2}\,\Delta\beta\,H^2\,dZ(X_u - X_l) \tag{2}$$

where X_u and X_l are the upper and lower limits of the X-surface seen by the receiver, as shown in figure 2. Some of the power being emitted from surface Y may be reflected from surface X in the direction of the receiver. In figure 2, the first image of Y is drawn as n = 1. The power arriving at the receiver from surface Y after one reflection can now be assumed to be coming directly from this image with its intensity reduced by the amount that would be absorbed in one reflection. This power can be written as

$$Q_{1,X-\Delta R} = (1 - \epsilon_w) q_w \frac{\cos \beta_1}{2} \Delta\beta_1 H^2 \, dZ(X_{u,1} - X_{l,1}) \tag{3}$$

where $X_{u,1}$ and $X_{l,1}$ are the upper and lower limits of the beam from image 1, and β_1 is shown in figure 2.

Also, some of the power being emitted from surface X is reflected from surface Y to surface X and then to the receiver. The X-surface image emitting the power in this sequence is denoted by $n = 2$. In a like manner, images of both X- and Y-surfaces for greater numbers of reflections are shown. If n is even, the corresponding image is of the X-surface; and if n is odd, the image of the Y-surface:

$$Q_{n,X-\Delta R} = (1 - \epsilon_w)^n \, q_w \frac{\cos \beta_n}{2} \Delta\beta_n H^2 \, dZ(X_{u,n} - X_{l,n}) \tag{4}$$

It can be determined geometrically from figures 1 and 2 that

$$\beta_n = \beta - n\theta \tag{5}$$

From figure 2, for those wall images whose emission completely covers the field of view of the receiver, the upper and lower limits are

$$X_{u,n} = \frac{\cos \beta}{\cos \theta \cos(\beta - n\theta)} \tag{6a}$$

$$X_{l,n} = \frac{\cos(\theta + \beta)}{\cos(\beta - n\theta)} \tag{6b}$$

However, for those images whose emission covers only part of the field of view, that is, when

$$\frac{\cos \beta}{\cos \theta \cos(\beta - n\theta)} > I_n \tag{7}$$

where

$$I_n = \begin{cases} \dfrac{1}{\cos \theta}; & n = 0,2,4, \ldots \\ 1; & n = 1,3,5, \ldots \end{cases} \tag{8}$$

$X_{u,n}$ must equal I_n. The last image viewed by the receiver can be defined as N. For this case, I_n is given by the largest value N that satisfies the inequality

$$I_N > \frac{\cos(\theta + \beta)}{\cos(\beta - N\theta)} \tag{9}$$

The field of vision of the receiver does not intercept any further images, and no further energy is incident on the receiver after the N^{th} term. The terms

are summed up to the N^{th} term to obtain the net heat emitted to the receiver, or

$$Q_{X-\Delta R} = \sum_{n=0}^{N} Q_{n,X-\Delta R}$$

As pointed out before, these results apply when $\pi/2 - \theta \geq \beta > -\theta$, that is, when none of the Y-surface is seen by the receiver. Instead of β, an angle η may be defined as the angle between the normal to the base plane and the outgoing beam in the direction of the receiver, as shown in figure 1, and is

$$\eta = \theta + \beta - \frac{\pi}{2} \tag{10a}$$

These results would then apply when

$$0 \geq \eta > -\frac{\pi}{2} \tag{10b}$$

Side Y Directly Visible to Receiver

For the case when none of side X is visible to the receiver, η must be in the range

$$\frac{\pi}{2} > \eta \geq \theta \tag{11}$$

as can be seen in figure 3. The power reaching the receiver from surface Y is

$$Q_{0,Y-\Delta R} = q_w \frac{\cos \psi}{2} \Delta\psi \, H^2 \, dZ(Y_u - Y_l) \tag{12}$$

where ψ is the angle between the normal to the Y-surface and the emitted beam and is given by

$$\psi = \eta - \frac{\pi}{2} \tag{13}$$

The power being emitted to the receiver from the n^{th} image can be seen from figure 3 to be

$$Q_{n,Y-\Delta R} = (1 - \epsilon_w)^n \, q_w \frac{\cos \psi_n}{2} \Delta\psi_n H^2 \, dZ(Y_{u,n} - Y_{l,n}) \tag{14}$$

Figures 1 and 3 show that

$$\psi_n = \psi + n\theta \tag{15}$$

$$Y_{u,n} = \frac{\cos \psi}{\cos(\psi + n\theta)} \tag{16}$$

$$Y_{l,n} = \frac{\cos(\psi - \theta)}{\cos \theta \cos(\psi + n\theta)} \tag{17}$$

As in the case for the X-surface, when

$$\frac{\cos \psi}{\cos(\psi + n\theta)} > I_{n+1}$$

then

$$Y_{u,n} = I_{n+1} \tag{18}$$

and the series stops at term M, where M is the largest value that satisfies the inequality,

$$I_{M-1} > \frac{\cos(\psi - \theta)}{\cos \theta \cos(\psi + M\theta)} \tag{19}$$

Both Sides X and Y Visible to Receiver

For this case, η must be in the range

$$\theta > \eta > 0 \tag{20}$$

The path of the beam for this case is shown by dashed lines in figures 2 and 3. The emitted power to the receiver can be considered to come, in part, from the X-surface and in part from the Y-surface. The power emitted to the receiver from the X-surface, after n reflections, is given by equation (4), where $X_{l,n} = 0$; and equations (5), (6a), and (7) still apply. The series will stop for $n = N$ where $N < [(\pi + \eta - \theta)_{\theta}] < N + 1$, because then the angle between side Y and the image $N + 1$ in a clockwise direction becomes greater than the angle between side Y and the lower limit of the beam after it passes through the vertex as in figure 2. Then the power emitted from image $N + 1$ will not be seen by the receiver. The power to the receiver from the Y-surface emitted from image n is given by equation (14) with $Y_{l,n} = 0$, and equations (15), (16), and (18) still apply. This series stops when $n = M$, where $M < \frac{\pi - \eta}{\theta} < M + 1$, as can be seen from figure 3, and was explained in the previous case.

Comparison with Flat, Black Surface

These results were compared with the emission from a flat, black surface of area equal to the base of one groove. For this case, the total energy reaching

over the groove. The rate of energy per unit area leaving the emitter diffusely is q_E. Again the problem can be divided into three cases: (1) Side X directly visible to the emitter, (2) Side Y directly visible to the emitter, and (3) both sides X and Y directly visible to emitter.

Side X Directly Visible to Emitter

The power reaching side X directly from the emitter when

$$0 \geq \eta' > -\frac{\pi}{2} \tag{22}$$

as can be seen in figure 2 where β is replaced by β', is

$$Q_{\Delta E-X} = q_E \frac{\cos \beta'}{2} \Delta\beta' H^2 dZ(X_{u'} - X_{l'}) \tag{23a}$$

The angle η' is the angle between the normal to the base plane and the incident beam as shown in figure 1. Use was made of the reciprocal relation between shape factors $A_1F_{1-2} = A_2F_{2-1}$ in obtaining equation (23a). This is clearly equal to the power that would be incident on an element of the base plane with an area equal to the base of one groove. Thus,

$$Q_{\Delta E-X} = Q_{\Delta E-\Delta\xi} = q_E \frac{\cos \eta'}{2} \Delta\eta' \, dZ \, H^2 \tan \theta$$

This will be reflected all or in part at a lower intensity to wall Y. Again, the image of wall Y can be drawn as $n = 1$. The whole beam will continue to be reflected until

$$\frac{\cos \beta'}{\cos \theta \cos(\beta' - n'\theta)} > I_{n'} \tag{23b}$$

where n' denotes the image where the incident beam is not intercepted completely but a part leaves the groove (fig. 2). The part of the energy reflected off image $n' - 1$ and out into the environment is equal to some fraction of the attenuated incident beam:

$$Q_{n'-1,\Delta E-X} = f_{X,n'-1}(1 - \epsilon_w)^{n'} Q_{\Delta E-X} \tag{24}$$

The fraction of the unattenuated whole beam that will be reflected off image n and out of the groove is defined as f_n. Dividing by the magnitude of the incident radiation yields the directional reflectivity, which can be written as

$$(\rho_{\eta',\eta})_{n'-1} = \frac{Q_{n'-1,\Delta E-X}}{Q_{\Delta E-\Delta\xi}} = f_{X,n'-1}(1 - \epsilon_w)^{n'} \tag{25}$$

where

the receiver is

$$Q_{b,\Delta\xi-\Delta R} = q_b \, dZ \, H^2 \tan\theta \cos\eta \, \frac{\Delta\eta}{2}$$

where $\Delta\xi$ is the groove-base width and is equal to $H \tan\theta$. Dividing the emitted energy from the groove by the energy emitted from the black surface and defining this ratio as ϵ_η yield the equations given previously, which can be summarized as follows:

$$\epsilon_\eta = -\frac{\epsilon_w}{\tan\theta \cos\eta}\left(\sum_{n=0}^{N}\left\{(1-\epsilon_w)^n \sin[\eta-(n+1)\theta](X_{u,n}-X_{l,n})\right\}\right.$$

$$\left. -\sum_{n=0}^{M}\left[(1-\epsilon_w)^n \sin(\eta+n\theta)(Y_{u,n}-Y_{l,n})\right]\right) \qquad (21)$$

where N and M are the maximum values of n considered in their respective series.

(1) For $0 \geq \eta > -\pi/2$:

$Y_{u,n} = Y_{l,n}$; $X_{u,n}$ is given by equations (6a) and (7); $X_{l,n}$ by equation (6b). The series stops for $n = N$, as given by equation (9).

(2) For $\pi/2 > \eta \geq \theta$:

$X_{u,n} = X_{l,n}$; $Y_{u,n}$ is given by equations (16) and (18); $Y_{l,n}$ by equation (17). The series stops for $n = M$, as given by equation (19).

(3) For $\theta > \eta > 0$:

$X_{l,n} = Y_{l,n} = 0$; $X_{u,n}$ and $Y_{u,n}$ are given in items (1) and (2). The series stop for N and M given by

$$N < \left(\frac{\pi+\eta-\theta}{\theta}\right) < N+1$$

$$M < \left(\frac{\pi-\eta}{\theta}\right) < M+1$$

DIRECTIONAL REFLECTION

In this section, the direction and magnitude of the reflection of an incident beam from a groove are analyzed. There is an emitter of width ΔE infinite in the Z-direction radiating to the groove. The angle between the normal to the surface X and the incident beam is β'. The emitter is far enough away compared with the lengths of H and L so that β' can be considered constant

$$f_{X,n'-1} = \frac{X_{u',n'-1} - \lambda_{X,n'-1}}{X_{u',n'-1} - X_{l',n'-1}} \tag{26}$$

and $\lambda_{X,n'-1}$ is shown in figure 2 and is equal to the inner boundary of the beam that is reflected from image $n' - 1$ and out of the groove.

The direction in which this beam will be reflected from the groove is $\eta_{X,n'-1}$ and can be obtained geometrically from figure 2 as:

$$\eta_{X,n} = \begin{cases} \pi + \eta' - (n + 1)\theta; & n = 1,3,5 \ldots \\ -\eta' - \pi + (n + 2)\theta; & n = 0,2,4, \ldots \end{cases} \tag{27}$$

If

$$\frac{\cos(\theta + \beta)}{\cos(\beta' - n'\theta)} > I_{n'}$$

then

$$\lambda_{X,n'-1} = \frac{\cos(\theta + \beta')}{\cos[\beta' - (n' - 1)\theta]}$$

and this will be the only beam reflected from the groove. Otherwise, it can be seen geometrically and by use of equation (6a) that

$$\lambda_{X,n'-1} = I_{n'} \frac{\cos(\beta' - n'\theta)}{\cos[\beta' - (n' - 1)\theta]} \tag{28}$$

The directional reflectivity of the next beam that will be reflected from the groove is

$$(\rho_{\eta',\eta})_{n'} = f_{X,n'}(1 - \epsilon_w)^{n'+1} \tag{29a}$$

where

$$f_{X,n'} = \frac{I_{n'} - \lambda_{X,n'}}{X_{u',n'} - X_{l',n'}} \tag{29b}$$

If

$$\frac{\cos(\theta + \beta')}{\cos[\beta' - (n' + 1)\theta]} > I_{n'+1} \tag{30}$$

then

$$\lambda_{X,n'} = \frac{\cos(\theta + \beta')}{\cos(\beta' - n'\theta')}$$

and this will be the last beam radiated from the groove. Otherwise,

$$\lambda_{X,n'} = I_{n'+1} \frac{\cos[\beta' - (n' + 1)\theta]}{\cos(\beta' - n'\theta)}$$

In this case, the direction of the emitted beam is $\eta_{X,n'}$.

The directional reflectivity of the next beam can be obtained similarly as

$$(\rho_{\eta',\eta})_{n+1} = f_{X,n'+1}(1 - \epsilon_w)^{n'+2} \tag{31a}$$

where

$$f_{X,n'+1} = \frac{I_{n'+1} - \lambda_{X,n'+1}}{X_{u',n'+1} - X_{l',n'+1}} \tag{31b}$$

If

$$\frac{\cos(\theta + \beta')}{\cos[\beta' - (n' + 2)\theta]} > I_{n'+2} \tag{32}$$

then

$$\lambda_{X,n'+1} = \frac{\cos(\theta + \beta')}{\cos[\beta' - (n' + 1)\theta]}$$

and this is the last beam reflected from the groove. Otherwise,

$$\lambda_{X,n'+1} = I_{n'+2} \frac{\cos[\beta' - (n' + 2)\theta]}{\cos[\beta' - (n' + 1)\theta]}$$

The direction of the emitted beam leaving the groove is now $\eta_{X,n'+1}$. This procedure is carried on until

$$\frac{\cos(\theta + \beta')}{\cos(\beta' - n\theta)} > I_n$$

Side Y Directly Visible to Emitter

The energy reaching side Y directly from the emitter for the case when $\pi/2 > \eta' \geq \theta$, as illustrated in figure 3, with the angle symbols now primed to denote the incident beam case, is

$$Q_{\Delta E-Y} = q_E \frac{\cos \psi'}{2} \Delta\psi' \, H^2 \, dZ(Y_{u'} - Y_{l'})$$

$$= q_E \frac{\cos \eta'}{2} \Delta\eta' \, dZ \, H^2 \tan \theta \tag{33}$$

The equation for ψ' is given by equation (13), with η replaced by η'. This is also the energy that would be incident on an element of the base plane of area equal to the base of the groove, as written in the second equality of equation (33).

As seen in figure 3, the whole incident beam will be reflected internally until

$$\frac{\cos \psi}{\cos(\psi + n'\theta)} > I_{n'+1} \tag{34}$$

where $I_{n'+1}$ is the length of the n' image and $Y_{u',n'}$ and $Y_{l',n'}$ are given by equations (16) and (17), respectively, with ψ replaced by ψ'. The part of the attenuated incident beam that will emerge divided by the incident radiation given by equation (33) is

$$(\rho_{\eta',\eta})_{n'-1} = f_{Y,n'-1}(1 - \epsilon_w)^{n'} \tag{35a}$$

where

$$f_{Y,n'-1} = \frac{Y_{u',n'-1} - \lambda_{Y,n'-1}}{Y_{u',n'-1} - Y_{l',n'-1}} \tag{35b}$$

If

$$\frac{\cos(\psi - \theta)}{\cos \theta \cos(\psi + n'\theta)} > I_{n'-1}$$

then

$$\lambda_{Y,n'-1} = \frac{\cos(\psi - \theta)}{\cos \theta \cos[\psi + (n' - 1)\theta]}$$

and this will be the last emerging beam. Otherwise, it can be shown from figure 3 and equation (16) that

$$\lambda_{Y,n'-1} = \frac{\cos(\psi + n'\theta)}{\cos[\psi + (n' - 1)\theta]} I_{n'+1} \tag{36}$$

The direction of the reflected beam from the groove is $\eta_{Y,n'-1}$ where

$$\eta_{Y,n} = \begin{cases} -\eta' - n\theta + \pi & n = 0,2,4,6, \ldots \\ \eta' - \pi + (n + 1)\theta; & n = 1,3,5, \ldots \end{cases} \tag{37}$$

The directional reflectivity of the next beam reflected from the groove is

$$(\rho_{\eta',\eta})_{n'} = f_{Y,n'}(1 - \epsilon_w)^{n'+1} \tag{38}$$

where

$$f_{Y,n'} = \frac{I_{n'-1} - \lambda_{Y,n'}}{Y_{u',n'} - Y_{l',n'}} \tag{39}$$

Again, if

$$\frac{\cos(\psi - \theta)}{\cos\theta \cos[\psi + (n' + 1)\theta]} > I_{n'}$$

then

$$\lambda_{Y,n'} = \frac{\cos(\psi - \theta)}{\cos\theta \cos(\psi + n'\theta)}$$

and no further beams will be reflected from the groove. Otherwise,

$$\lambda_{Y,n'} = \frac{\cos[\beta' + (n' + 2)\theta]}{\cos[\beta' + (n' + 1)\theta]} I_{n'} \tag{40}$$

The direction of this beam will be $\eta_{Y,n'}$.

The next beam reflected from the groove would have directional reflectivity

$$(\rho_{\eta',\eta})_{n'+1} = f_{Y,n'+1}(1 - \epsilon_w)^{n'+2} \tag{41}$$

where

$$f_{Y,n'+1} = \frac{I_{n'} - \lambda_{Y,n'+1}}{Y_{u',n'+1} - Y_{l',n'+1}} \tag{42}$$

If

$$\frac{\cos(\psi - \theta)}{\cos\theta \cos[\psi + (n' + 2)\theta]} > I_{n'+1}$$

then

$$\lambda_{Y,n'+1} = \frac{\cos(\psi - \theta)}{\cos\theta \cos[\psi + (n' + 1)\theta]}$$

and no further beams will be reflected from the groove. Otherwise,

$$\lambda_{Y,n'+1} = \frac{\cos[\beta' + (n' + 3)\theta]}{\cos[\beta' + (n' + 2)\theta]} I_{n'+1} \tag{43}$$

The direction of this beam is $\eta_{Y,n'+1}$. The procedure is carried on in this manner until

$$\frac{\cos(\psi - \theta)}{\cos\theta \cos(\psi + n\theta)} > I_{n'+1}$$

Both Sides X and Y Visible to Emitter

For the case in which the incoming beam is between the angles $\theta > \eta' > 0$, both sides of the groove are illuminated. In this case, the problem is divided into two parts, as illustrated by the dashed lines in figures 2 and 3.

The power reaching side X is given by

$$Q_{\Delta E,X} = q_E \frac{\cos\beta'}{2} \Delta\beta' H^2 dZ X_{u'} \tag{44a}$$

The part of this beam emerging from the groove is

$$Q_{n'-1,\Delta E-X} = f_{X,n'-1} \frac{X_{u',n'-1} - X_{l',n'-1}}{X_{u',n'-1}} (1 - \epsilon_w)^{n'} Q_{\Delta E-X} \tag{44b}$$

If equation (44b) is divided by the value of the total incident radiation, which is given by equation (23a), the following result is obtained:

$$(\rho_{\eta',\eta})_{n'-1} = f_{X,n'-1} (1 - \epsilon_w)^{n'} \frac{(X_{u',n'-1} - X_{l',n'-1})}{X_{u',n'-1}} \frac{X_{u'}}{(X_{u'} - X_{l'})} \tag{44c}$$

which reduces to equation (25). Equations (26) to (28) still apply. Each term is calculated as before, except that the test to determine the last beam is changed. The terms are found until the N' beam is reached, where N' is determined from

$$N' < \frac{(\pi + \eta' - \theta)}{\theta} < N' + 1 \tag{44d}$$

This relation is the same as that obtained in the emission solution for the case where $\theta > \eta > 0$, with η replaced by η'. The image N' + 1 is the first image not in the path of the incident beam, as shown in figure 2; then $X_{l',N'} = 0$, and there are no further beams reflected from the groove. For the Y-part, a similar procedure is followed. Again, equations (35) to (43) apply except for the test for the final beam. The beams reflected from the groove are found until the M' beam for which $Y_{l',M'} = 0$, where M' is determined from

$$M' < \left(\frac{\pi - \eta'}{\theta}\right) < M' + 1 \tag{45}$$

as in the emission solution. The image M' + 1 is again the first image not in the path of the incident beam, as seen in figure 3.

RESULTS AND DISCUSSION

Emission Results

The directional emissivity for some representative cases is plotted in figure 4. The radial coordinate ϵ_η is the energy emitted from one groove at an angle η from the normal of the base plane divided by the energy that would be emitted in that same direction by a black surface of area equal to the base of the groove. The angle θ between the groove walls and the emissivity of the wall material ϵ_w are shown as parameters.

The directional emissivity tends to peak at $\eta = \theta/2$. The value of ϵ_η at this angle is much higher than the wall emissivity ϵ_w. The smaller the angle θ between the groove walls, the closer the directional emissivity approaches that of a black body for the range $0 < \eta < \theta$. For large open angles of θ this effect is not as pronounced, and for θ of 75° the peak directional emissivity occurs at an η higher than $\theta/2$. This phenomenon is a result of the large specular reflection of the radiation from the diagonal wall off the wall normal to the base plane.

For η of large negative values, where the receiver sees only the tip of the diagonal surface, the directional emissivity is the same as the wall material ϵ_w, because there is no additional reflected radiation in that direction.

For large positive values of η, the curve of ϵ_η tends to be constant at a value higher than the wall emissivity because of the geometry chosen, which causes at least one wall image to emit to the receiver.

Figure 5 shows the result of multiplying certain of the curves in figure 4 by $\cos \eta$. This operation gives the radiation emitted in the direction η compared with the radiation emitted normal to the base plane by a black surface of area equal to the base of the groove. It can be seen that the angle of peak emission is shifted away from $\eta = 0^\circ$.

Reflection Results

The directional reflectivity $\rho_{\eta',\eta}$ for a fixed wall emissivity ϵ_w of 0.1 is plotted in figure 6. These results are shown for various angles of groove opening θ.

The labeling of these curves can be explained by looking at figure 6(c). The radial scale from 0 to 1.0, labeled $\rho_{\eta',\eta}$, is the magnitude of the reflected beam divided by the magnitude of the incident beam for one groove. The outer angular scale labeled η is the angle of the reflected beam. The inner angular scales labeled (η',X1), (η',Y2), and so forth, denote the angle of the incident beam η'. The X1 refers to the solid curve 1 and signifies that the reflected radiation is from a beam incident on the X-surface. The 1 means the number of times the beam is reflected before it emerges from the groove. The Y2 refers to the dashed curve 2 and signifies that the reflected radiation is from a beam

incident on the Y-surface. The 2 means the number of reflections the incident beam underwent before it emerged.

As an example, for an incident angle of η' between -90° and -30°, the entire beam will emerge in the direction η between 30° and -30° after one reflection. The label (η',X1) refers to the incident beam from angle η', which illuminates surface X and emerges after one reflection. For an incident angle of η' between -30° and 0°, two beams will emerge from the groove (fig. 6(c)), since this range of incident angles can be found in both (η',X1) and (η',X2). This is true because part of the beam reflected from the X-surface is intercepted by the Y-surface. This part emerges from the groove after two reflections with a reduction in power due to absorption in the additional reflection. The remainder is reflected out directly.

For incident beams with η' between 0° and 30°, part of the beam is reflected directly, part after two reflections, and the remainder after three reflections, as is shown by the η' in this range that appears on the (η',X1) (η',X2), and (η',X3) scales. The radiation incident on the X-surface from η' of 30° to 60° will be reflected out only after three reflections, as shown by the fact that this range appears only on the (η',X3) scale. For η' from 60° to 90° there will be no radiation incident on the X-surface.

If the incident beam on the Y-surface is now considered for η' of 60° to 90°, as shown on the scale (η',Y2), it can be seen from curve 2 that the entire beam will be radiated out of the groove after two reflections in the direction η from 0° to 30°, respectively. For a beam of η' between 30° and 60°, only part of the beam will radiate out after two reflections. The rest will emerge after three reflections, indicated by this range of η' that appears on the (η',Y2) and (η',Y3) scales. The power incident on the Y-surface for η' between 30° and 0° will emerge from the groove only after three reflections. For η' less than 0°, no beam is incident on the Y-surface.

To illustrate the use of the curves, the reflected beams from an incident beam with $\eta' = 15^\circ$ are shown in figure 6(c). The magnitude and direction of each emerging beam are shown by the four outward pointing arrows. One in the direction $\eta = -75^\circ$ with a magnitude of 0.241 emerges after one reflection. Another part of the incident beam is reflected in the direction $\eta = 75^\circ$ with a magnitude of 0.217. This beam emerges after two reflections. Finally, there are two beams at $\eta = 45^\circ$ with magnitudes of 0.226 and 0.113. These will be radiated out after three reflections. The sum of these reflected beams is 0.797. The value of the directional emissivity ϵ_η is 0.203 for the same groove parameters considered in the preceding example and for an η of 15°. As shown and discussed subsequently, the directional absorptivity $\alpha_{\eta'}$ is equal to the directional emissivity $\epsilon_{\eta'}$, where $\epsilon_{\eta'}$ is the emissivity in the direction of the incident radiation. Then the sum of the reflectivities $\sum_{\eta} \rho_{\eta',\eta}$ plus the emissivity $\epsilon_{\eta'}$ is 1.0. This relation was used to check the numerical calculations and is shown to be true in the previous example.

Figure 6 shows the effect of groove-wall angle θ. For larger values of θ, there are fewer internal reflections. When θ approaches the limiting value of

90°, the surface approaches the behavior of a flat mirror, as shown in figure 6(a) for θ of 89.9°. As θ decreases, there are more internal reflections causing greater absorption of the incident radiation and a larger number of reflected beams from a given incident beam, which is shown for θ of 30° in figure 6(b). For very small angles of θ, the incident beam is almost completely absorbed as a result of the many internal reflections, except for η' approaching 90°. For these cases, the reflected beams will be in a direction η close to $\pm 90^{\circ}$, as shown in figure 6(a) for a θ of 1°.

In figure 7, the groove geometry is the same as in figure 6(b). The wall emissivity is now $\epsilon_w = 0.01$ rather than 0.1, which results in curves similar in shape but greater in magnitude than those in figure 6(b).

DIRECTIONAL ABSORPTIVITY

The directional absorptivity $\alpha_{\eta'}$ can be shown to be equal to the directional emissivity ϵ_{η} when η' is equal to η for any isothermal cavity as follows: An isothermal enclosure with black walls is shown in figure 8. Disregarding dA_{B2}, there is within the enclosure a black elemental surface of area dA_{B1} and another body containing a cavity of arbitrary shape and an aperture of area dA_C. The radiative characteristics of the internal surface of the cavity are arbitrary. All bodies and surfaces are at temperature T. The radiation emitted from the black element and absorbed by the cavity is

$$Q_{B1-C} = \alpha_{C,\eta} q_b \, d^2F_{B1-C} \, dA_{B1} \tag{46}$$

where d^2F_{B1-C} is the shape factor from the element to the cavity aperture. The energy emitted from the isothermal cavity and absorbed by the black element is

$$Q_{C-B1} = \epsilon_{C,\eta} q_b \, d^2F_{C-B1} \, dA_C \tag{47}$$

which can be written as

$$Q_{C-B1} = \epsilon_{C,\eta} q_b \, d^2F_{B1-C} \, dA_{B1} \tag{48}$$

by using the reciprocal rule for shape factors. From the second law of thermodynamics, no net heat can be transferred between these two bodies, since they are at the same temperature. Equating Q_{B1-C} to Q_{C-B1} gives

$$\epsilon_{C,\eta} = \alpha_{C,\eta} \tag{49}$$

This relation can be used to check the calculations for the grooves. The difference between the power of the incident beam from direction η' and the power of the sum of its reflected beams is the power absorbed by the groove, which can be written as

$$1 - \sum_{\eta} \rho_{\eta',\eta} = \alpha_{\eta'} \tag{50a}$$

From equation (49), this becomes

$$\epsilon_{\eta'} + \sum_{\eta} \rho_{\eta',\eta} = 1 \tag{50b}$$

which was used as a check of the numerical calculations.

RECIPROCAL RELATION FOR REFLECTIVITIES

The reflectivity of an isothermal cavity for a given beam path is related to the reflectivity of the cavity for a beam path in the opposite direction. This can be shown as follows: From figure 8 and as discussed previously, the power incident on the cavity aperture from black element dA_{B2} is

$$Q_{B2-C} = q_b \, dA_{B2} \, d^2F_{B2-C} = q_b \, d^2F_{C-B2} \, dA_C$$

A fraction $\rho_{\eta',\eta}$ of this is reflected to dA_{B1}. Following the opposite path, the power reflected to dA_{B2} from dA_{B1} is

$$q_b \, dA_{B1} \, d^2F_{B1-C}\rho_{\eta,\eta'} = q_b \, dA_C \, d^2F_{C-B1}\rho_{\eta,\eta'}$$

Since the two bodies are at the same temperature, there can be no net heat exchange. The direct interchanges between dA_{B1} and dA_{B2} are equal. It follows that the reflected interchanges must also be equal, and

$$\rho_{\eta',\eta} \, d^2F_{C-B2} = \rho_{\eta,\eta'} \, d^2F_{C-B1} \tag{51a}$$

which, for the grooved surfaces, becomes

$$\rho_{\eta',\eta} = \rho_{\eta,\eta'} \frac{\cos \eta}{\cos \eta'} \tag{51b}$$

ILLUSTRATIVE EXAMPLES FOR DIRECTIONALLY EMITTING SURFACES

The following example illustrates the advantages of using surfaces with directional radiative properties for energy absorbers. Consider two parallel planes of width DE infinite in length and separated by a distance D, as shown in figure 9. The emitting surface is black and at temperature T_b. The absorbing surface is at temperature T_w and has a directional absorptivity $\alpha_{\eta'}$. The effects of environment are neglected.

The net power removal from the absorbing surface to maintain a constant T_w is the difference between the absorbed and emitted powers. The rate of energy absorbed from the black surface is

$$Q_{\Xi,a} = \sigma T_b^4 \frac{\Delta Z}{2} D^2 \int_0^{\Xi} \left(\int_{\eta_1'}^{\eta_2'} \alpha_{\eta'} \cos \eta' \, d\eta' \right) d\xi \tag{52}$$

The angle η_1' and η_2' are the limiting angles shown in figure 9 and are

$$\eta_1' = -\arctan(\xi) \tag{53a}$$

$$\eta_2' = \arctan(\Xi - \xi) \tag{53b}$$

The power emitted from the absorbing surface is

$$Q_{\Xi,e} = T_w^4 \frac{D^2 \Delta Z}{2} \int_0^{\Xi} \left(\int_{-\pi/2}^{\pi/2} \epsilon_\eta \cos \eta \, d\eta \right) d\xi \tag{54}$$

The power that must be removed from the absorbing surface to maintain constant T_w divided by the emission from the black surface is

$$\frac{q_G}{q_b} = \frac{Q_G}{\sigma T_b^4 D^2 \Xi \, \Delta Z} = \left[1 - \left(\frac{T_w}{T_b} \right)^4 \right] \frac{1}{2\Xi} \int_0^{\Xi} \left(\int_{\eta_1'}^{\eta_2'} \alpha_{\eta'} \cos \eta' \, d\eta' \right) d\xi$$

$$- \frac{1}{2\Xi} \left(\frac{T_w}{T_b} \right)^4 \int_0^{\Xi} \left[\int_{-\pi/2}^{\eta_1'} + \int_{\eta_2'}^{\pi/2} (\epsilon_\eta \cos \eta \, d\eta) \right] d\xi \tag{55}$$

and q_G/q_b can be called the absorption factor.

In some cases, it is desirable to maximize the power absorbed by the absorbing surface. If T_w/T_b is less than one, the first term in equation (55) is always positive, while the second term is always negative. To maximize the energy absorbed, the positive term must be maximized, while the negative term must be minimized. This would be achieved if $\alpha_{\eta'}(\xi)$ were unity in the range $\eta_2'(\xi) > \eta' > \eta_1'(\xi)$ and zero for other angles. A surface with this absorptivity will be called a "perfect" absorber. A surface with characteristics approximating those of a "perfect" surface is analyzed in reference 7. The directional absorptivity for some ξ on such a surface is shown in figure 10. This results in a maximum possible absorption factor of

$$\left(\frac{q_G}{q_b}\right)_{max} = \frac{1}{\Xi}\left[1 - \left(\frac{T_w}{T_b}\right)^4\right]\left[(1 + \Xi^2)^{1/2} - 1\right] \tag{56}$$

For some grooved surfaces the directional absorptivity can be closely represented by a simple functional relation. The function $\alpha_{\eta'} = \epsilon_{\eta'} = 0.83 \cos \eta'$, as seen in figure 10, and labeled grooved emitter, closely approximates the directional emissivity for a θ of 1° and an ϵ_w of 0.01 as shown in figure 4(a). Using this relation in equation (55) yields an absorption factor of the form

$$\frac{q_G}{q_b} = \frac{0.83}{2}\left[\arctan \Xi - \left(\frac{T_w}{T_b}\right)^4 \frac{\pi}{2}\right] \tag{57}$$

For purposes of comparison, the absorption factor for a diffuse gray surface of absorptivity $\alpha_w = \epsilon_w$ is calculated and is

$$\frac{q_f}{q_b} = \frac{\epsilon_w}{\Xi}\left[(1 + \Xi^2)^{1/2} - 1 - \left(\frac{T_w}{T_b}\right)^4 \Xi\right] \tag{58}$$

A comparison of the absorption factors for these three types of surfaces is shown in figure 11. The dash-dot curves show the power that will be absorbed by a perfect absorber divided by the emission per unit area from the black emitting surface q_b. The solid curves show the power that would be absorbed by a grooved absorber divided by q_b. The dashed curves show the power that would be absorbed by a black surface divided by q_b. Multiplying the latter family of curves by α_w will give the absorption factor for a diffuse gray surface of that absorptivity.

The net heat absorbed by the perfect absorber is always positive, since its emissivity is zero to the cold environment. This is not true for the other two surfaces, where the power absorbed is negative for small values of Ξ, since these surfaces are then losing more heat to the environment than they are gaining from the emitting surface. The perfect absorber is always absorbing more heat than the other surfaces; however, for very large values of Ξ, the model approaches the case of radiant heat transfer between infinite planes. For the case of the diffuse surface, if its absorptivity is one, it will absorb as much heat as the perfect absorber. For an absorptivity less than one, the curves for the diffuse surface are reduced in magnitude by the factor α_w; and, thus, for large Ξ the diffuse surfaces would absorb less than the perfect absorber. The comparison of the diffuse absorber with the grooved absorber shows that for small Ξ the grooved absorber has a greater heat absorption, but this is reversed for the larger values of Ξ; however, since the diffuse solution must be multiplied by α_w, for small values of α_w, the grooved absorber can absorb more heat for large Ξ than the diffuse absorber.

To illustrate the advantage of surfaces with directional radiating properties in radiating energy directly to a heat sink, an example similar to the previous one may be used. By using figure 9 but now considering the directional surface to be at a higher temperature than the black surface, that is, $T_w/T_b > 1$, the directional surface will be emitting to the black surface. The

fraction of the net power supplied to the emitting surface that is incident on the heat sink can be calculated as follows: The net power being supplied to the emitting surface is given by equation (55). The net power incident on the black surface divided by the emission from the black surface is

$$\frac{Q_{b,G}}{\sigma T_b^4 \, \Delta Z \, D^2} = \frac{1}{2}\left(\frac{T_w}{T_b}\right)^4 \int_0^{\Xi} \left(\int_{\eta_1'}^{\eta_2'} \epsilon_{\eta'} \cos \eta' \, d\eta' \right) d\xi \tag{59}$$

Then the ratio of power incident on the black surface to the power supplied to the emitting surface is

$$\frac{Q_{bG}}{Q_G} = \frac{\left(\frac{T_w}{T_b}\right)^4 \int_0^{\Xi} \left(\int_{\eta_1'}^{\eta_2'} \epsilon_{\eta'} \cos \eta' \, d\eta' \right) d\xi}{\left(\frac{T_w}{T_b}\right)^4 \int_0^{\Xi} \left(\int_{-\pi/2}^{\pi/2} \epsilon_{\eta} \cos \eta \, d\eta \right) d\xi - \int_0^{\Xi} \left(\int_{\eta_1'}^{\eta_2'} \epsilon_{\eta'} \cos \eta' \, d\eta' \right) d\xi} \tag{60}$$

This can be maximized by using a perfect emitting surface to give

$$\left(\frac{Q_{bG}}{Q_G}\right)_M = \frac{1}{1 - \left(\frac{T_b}{T_w}\right)^4} \tag{61}$$

For the case of the grooved emitter, the ratio of power incident on the black surface to the power added to the grooved surface is

$$\frac{Q_{bG}}{Q_G} = \frac{\left(\frac{T_w}{T_b}\right)^4 \arctan \Xi}{\left[\frac{\pi}{2}\left(\frac{T_w}{T_b}\right)^4 - \arctan \Xi\right]} \tag{62}$$

The ratio of the power incident on the black surface to the power supplied to a diffusely emitting gray surface is

$$\frac{Q_{b,f}}{Q_f} = - \frac{\left(\frac{T_w}{T_b}\right)^4 \left[\left(1 + \Xi^2\right)^{1/2} - 1\right]}{\left[\left(1 + \Xi^2\right)^{1/2} - 1 - \left(\frac{T_w}{T_b}\right)^4 \Xi\right]} \tag{63}$$

A comparison of these three types of emitting surfaces is shown in figure 12. The dash-dot curves are the power incident on a black surface from a perfect emitter divided by the power supplied to the directional surface Q. The solid curves are the power incident on a black surface from a grooved emitter divided by Q. The dashed curves are the energy incident on a black surface from a diffuse surface divided by the power supplied to the flat surface.

The power incident on the black surface from the perfect emitter is seen always to be greater than for either of the other two surfaces for a given temperature ratio. Similarly, the power incident on the black surface is greater for the grooved emitter than for the diffuse surface for any given temperature and aspect ratio.

Equilibrium Temperature of Directionally Absorbing Surfaces

It would be of interest, in comparing the different types of surfaces as absorbers, to calculate the equilibrium temperatures of these surfaces with the assumption that no heat is added except by radiation. This equilibrium temperature $(T_w)_{eq}$ can be found from equation (55) by setting q_G equal to zero. This gives

$$\left(\frac{T_w}{T_b}\right)^4_{eq} = \frac{\displaystyle\int_0^{\Xi} \left(\int_{\eta_1'}^{\eta_2'} \epsilon_{\eta'} \cos \eta' \, d\eta' \right) d\xi}{\displaystyle\int_0^{\Xi} \left(\int_{-\pi/2}^{\pi/2} \epsilon_{\eta} \cos \eta \, d\eta \right) d\xi} \tag{64}$$

where the ratio of integrals is defined as the absorption efficiency. From equation (56), the absorption efficiency for the perfect absorber is

$$\left(\frac{T_w}{T_b}\right)^4_{eq} = 1 \tag{65}$$

For the grooved absorber from equation (57),

$$\left(\frac{T_w}{T_b}\right)^4_{eq} = \frac{2 \arctan \Xi}{\pi} \tag{66}$$

and for the gray diffuse absorber from equation (58),

$$\left(\frac{T_w}{T_b}\right)^4_{eq} = \frac{\left(1 + \Xi^2\right)^{1/2} - 1}{\Xi} \tag{67}$$

The absorption efficiencies for these surfaces are shown in figure 13. For the perfect absorber, the absorption efficiency is one for all values of Ξ. This means that the absorbing surface attains the same temperature as the emitter. The grooved absorber and the diffuse absorber have lower absorption efficiencies and, therefore, lower equilibrium temperatures for small Ξ but approach one for large Ξ. The grooved absorbers have higher absorption efficiencies than the diffuse absorbers.

CONCLUDING REMARKS

By this analysis, the large effect of small surface irregularities on the radiation characteristics of materials has been shown. Since the wavelengths for thermal radiation are very small, the size of the grooves that can cause these effects can also be very small. The present results show that there can be very significant differences between apparent properties and the actual properties of the material. Great care must be exercised in proper surface preparations when an attempt is made to measure radiative properties.

The results indicate that the directional radiative properties of surfaces can be controlled by design. It is possible, therefore, to increase the efficiency of radiation exchange by design of the local macroscopic surface structure.

It has also been shown that the directional emissivity of any isothermal cavity is equal to the directional absorptivity of the same cavity and that the reflectivity of the cavity for any path is related to the reflectivity of the cavity for radiation in the opposite path.

The idealized surface, the "perfect" absorber, can be closely simulated by a groove with perfectly reflecting specular walls and a black base, as is shown in reference 7.

Lewis Research Center
National Aeronautics and Space Administration
Cleveland, Ohio, April 18, 1963

REFERENCES

1. Eckert, E. R. G., and Drake, R. M.: Second ed., Heat and Mass Transfer. McGraw-Hill Book Co., Inc., 1959, p. 378.

2. Münch, Benjamin: Die Richtungsverteilung bei der Reflexion von Wärmestrahlung und ihr Einfluss auf die Wärmeübertragung. Mitteilung Nr. 16, Institut für Thermodynamik und Verbrennungsmotorenbau an der Eidgenössischen Technishen Hochschule, Zurich, Mar. 16, 1955.

3. Polyak, G. G.: Radiative Transfer Between Surfaces of Arbitrary Spatial Distribution of Reflexion. Radiative Trans. Proj. Trans. TT-9, Purdue Univ., 1961.

4. Dresser, D. L.: Elements of Solar Collector Design. Paper 61-24, Inst. Aero. Sci., 1961.

5. Eckert, E. R. G., and Sparrow, E. M.: Radiative Heat Exchange Between Surfaces with Specular Reflections. Int. Jour. Heat and Mass Transfer, vol. 3, 1961, pp. 42-54.

6. Jakob, Max: Heat Transfer. Vol. II. John Wiley & Sons, Inc., 1957.

7. Perlmutter, Morris, and Howell, John R.: A Strongly Directional Emitting and Absorbing Surface. (To be publ. in Jour. Heat Transfer.)

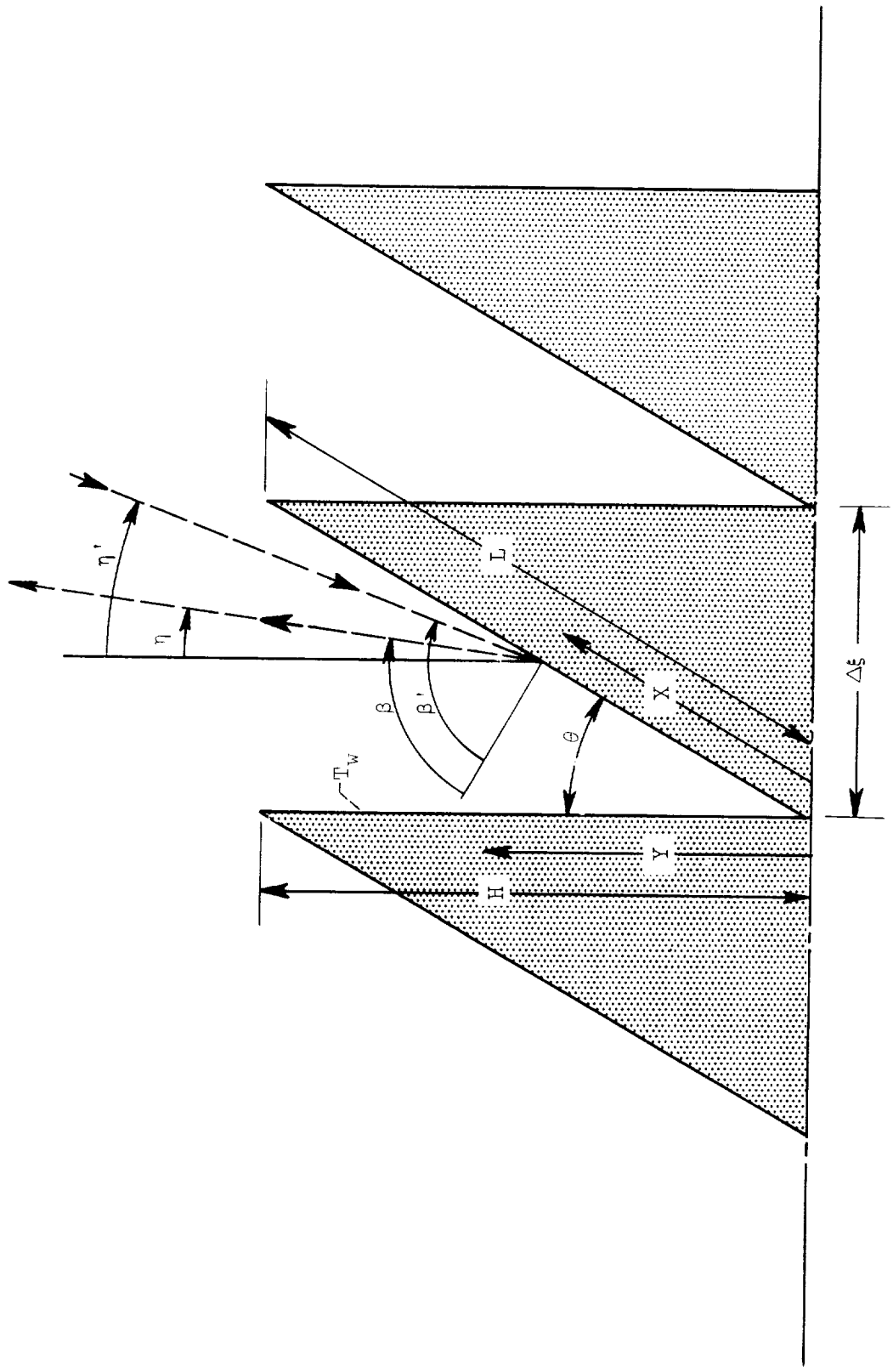

Figure 1. - Groove geometry.

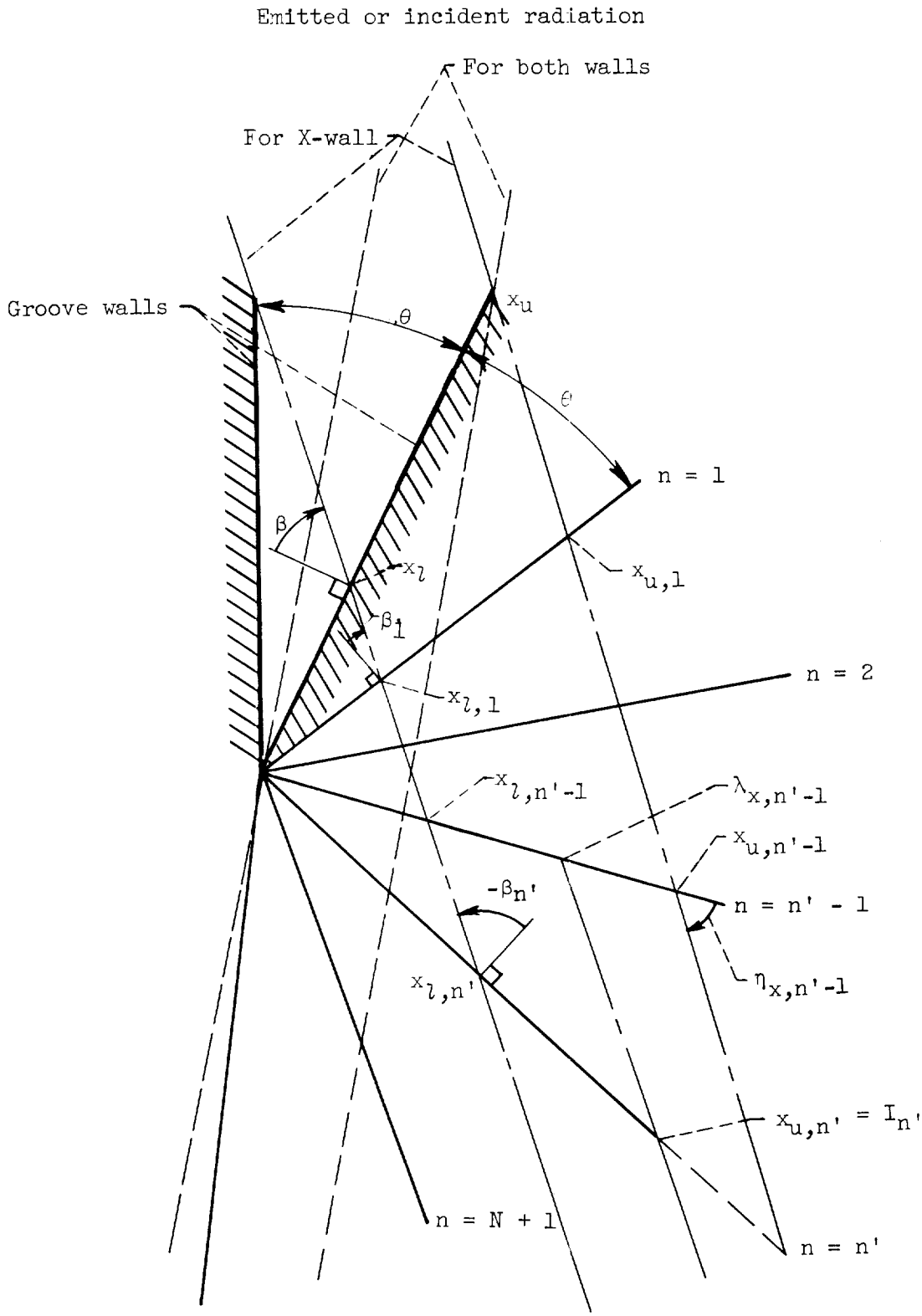

Figure 2. - Path of beam for diagonal surface.

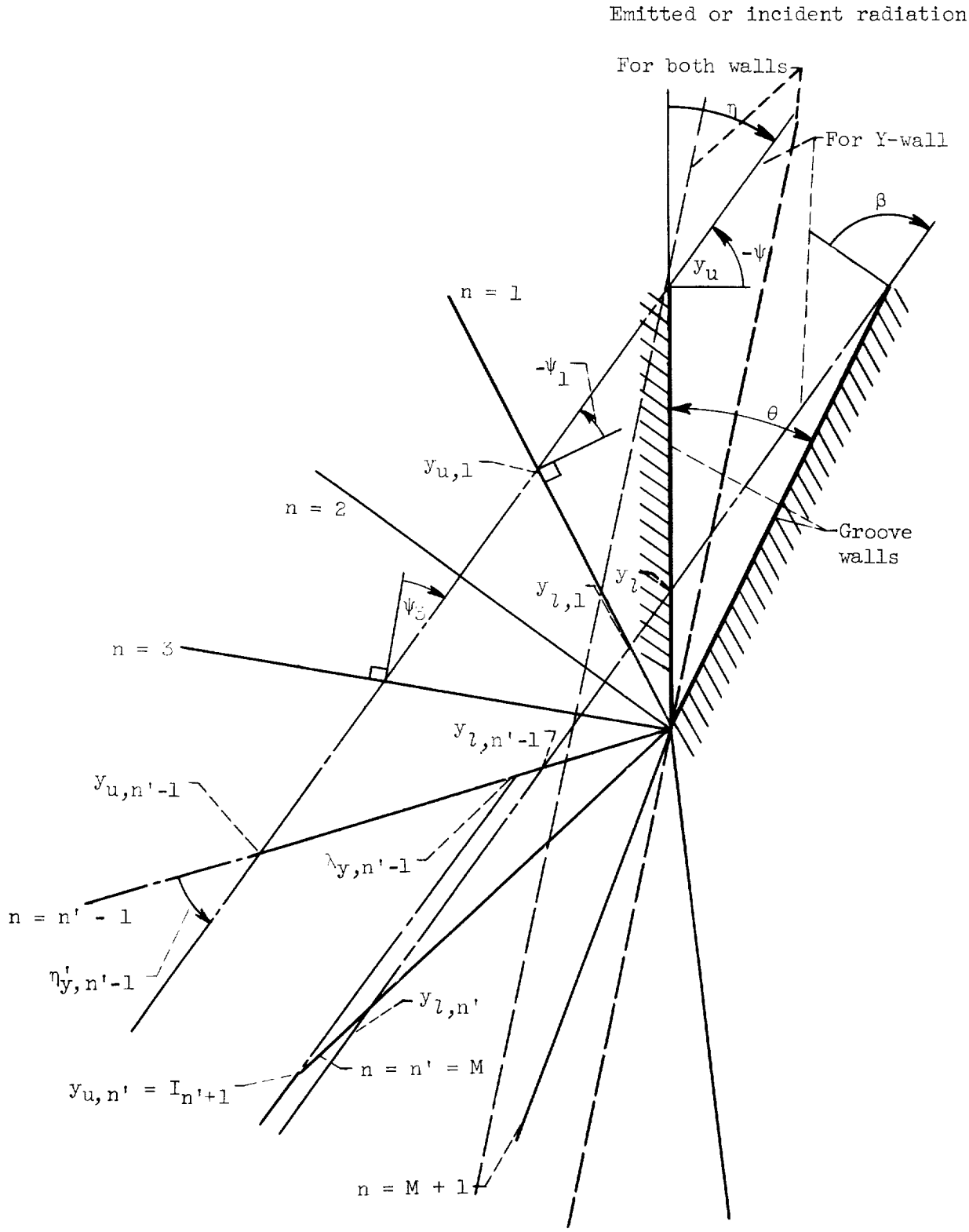

Figure 3. - Path of beam for Y-surface.

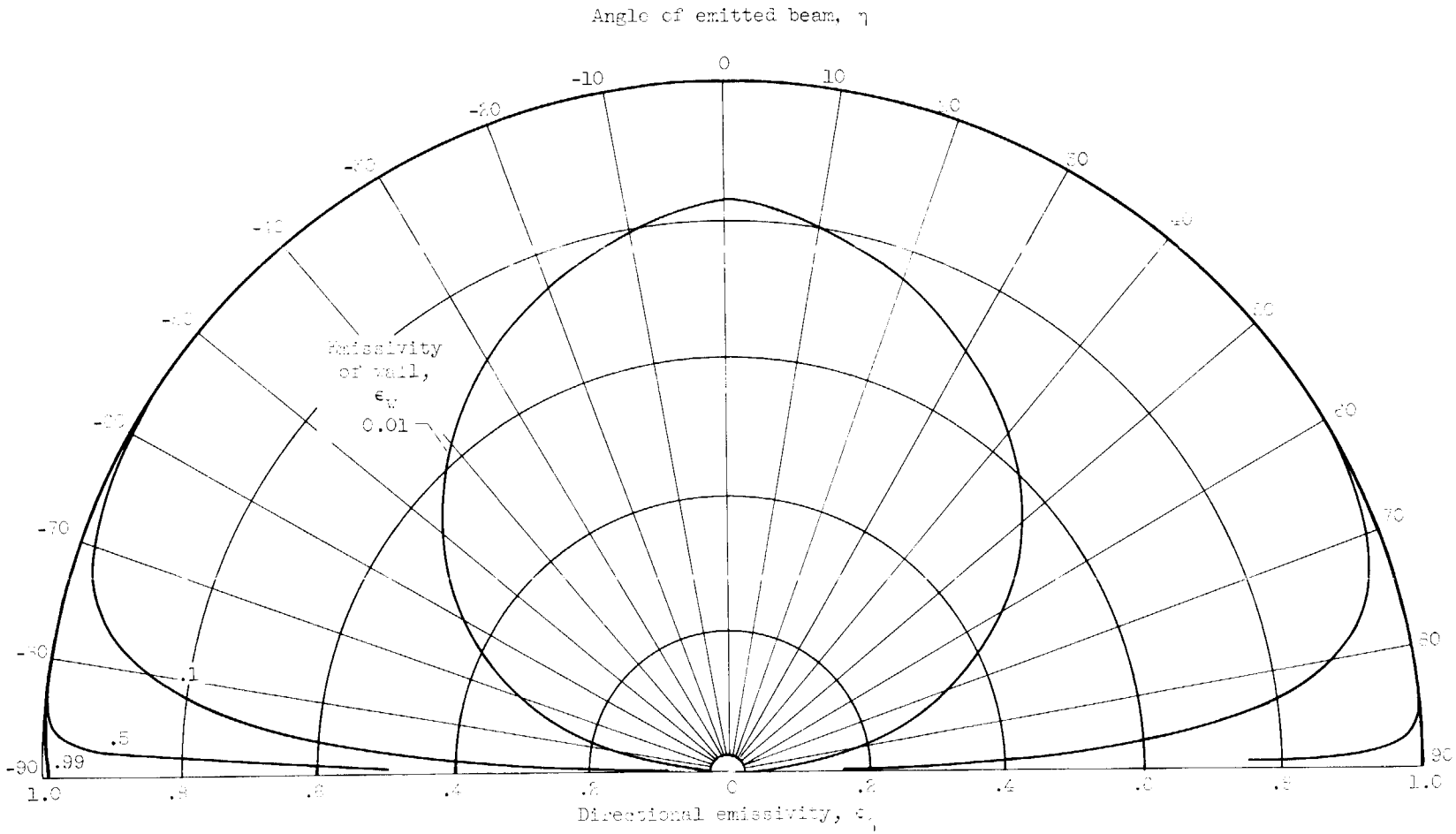

(a) Open angle between walls of groove, 1°.

Figure 4. - Directional emissivity of a grooved surface.

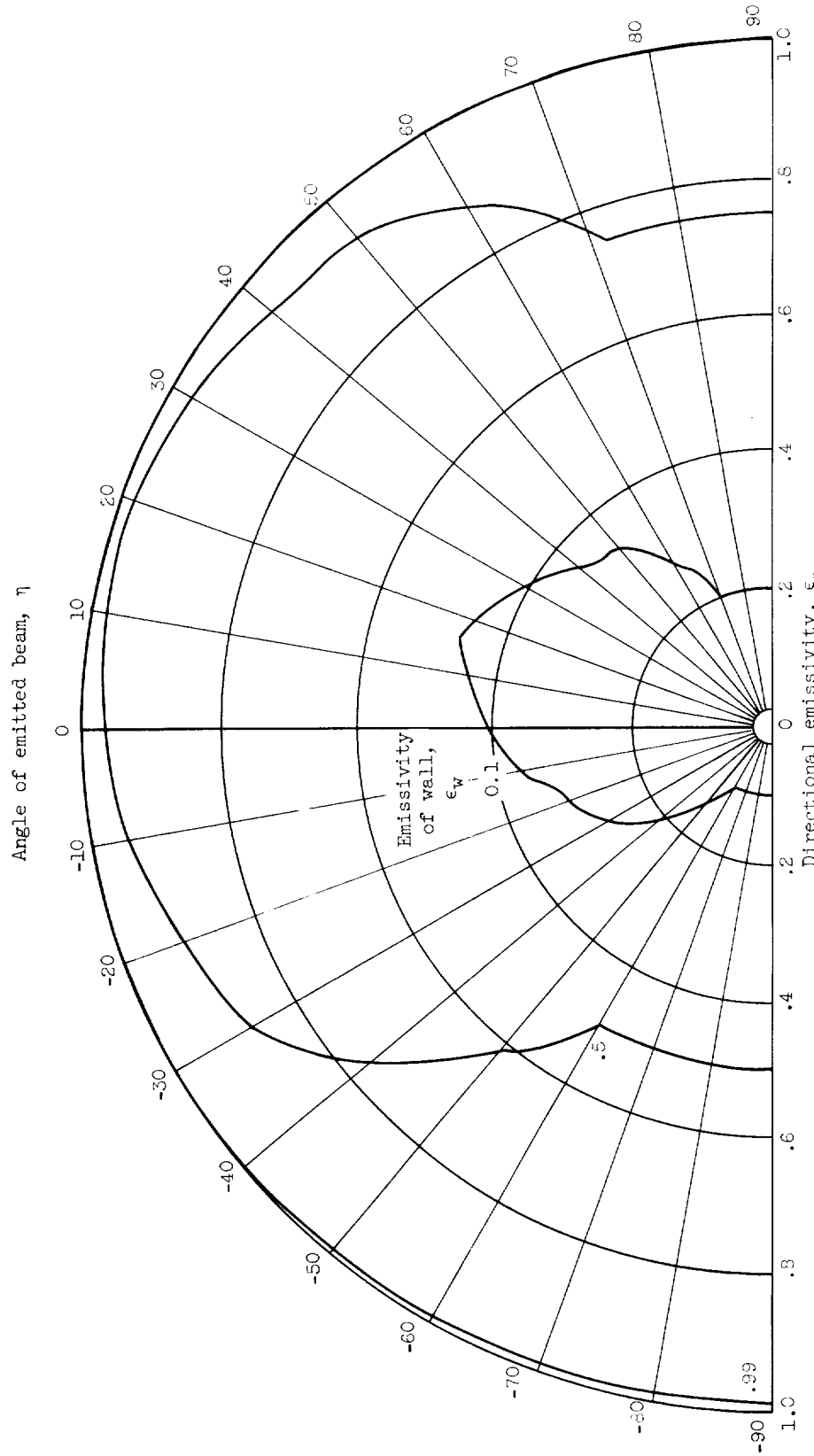

(b) Open angle between walls of groove, 30°.

Figure 4. - Continued. Directional emissivity of a grooved surface.

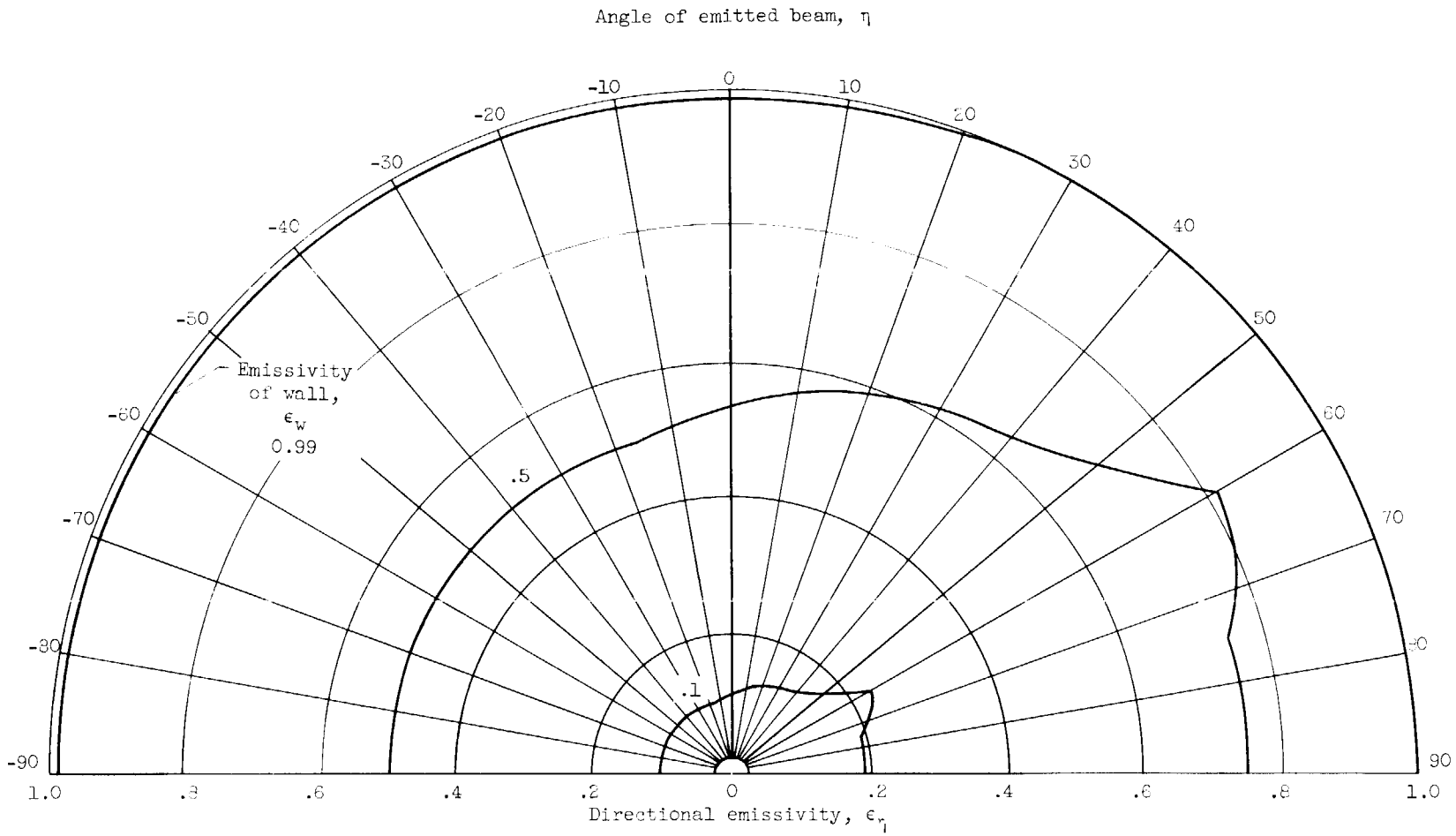

(c) Open angle between walls of groove, 75°.

Figure 4. - Concluded. Directional emissivity of a grooved surface.

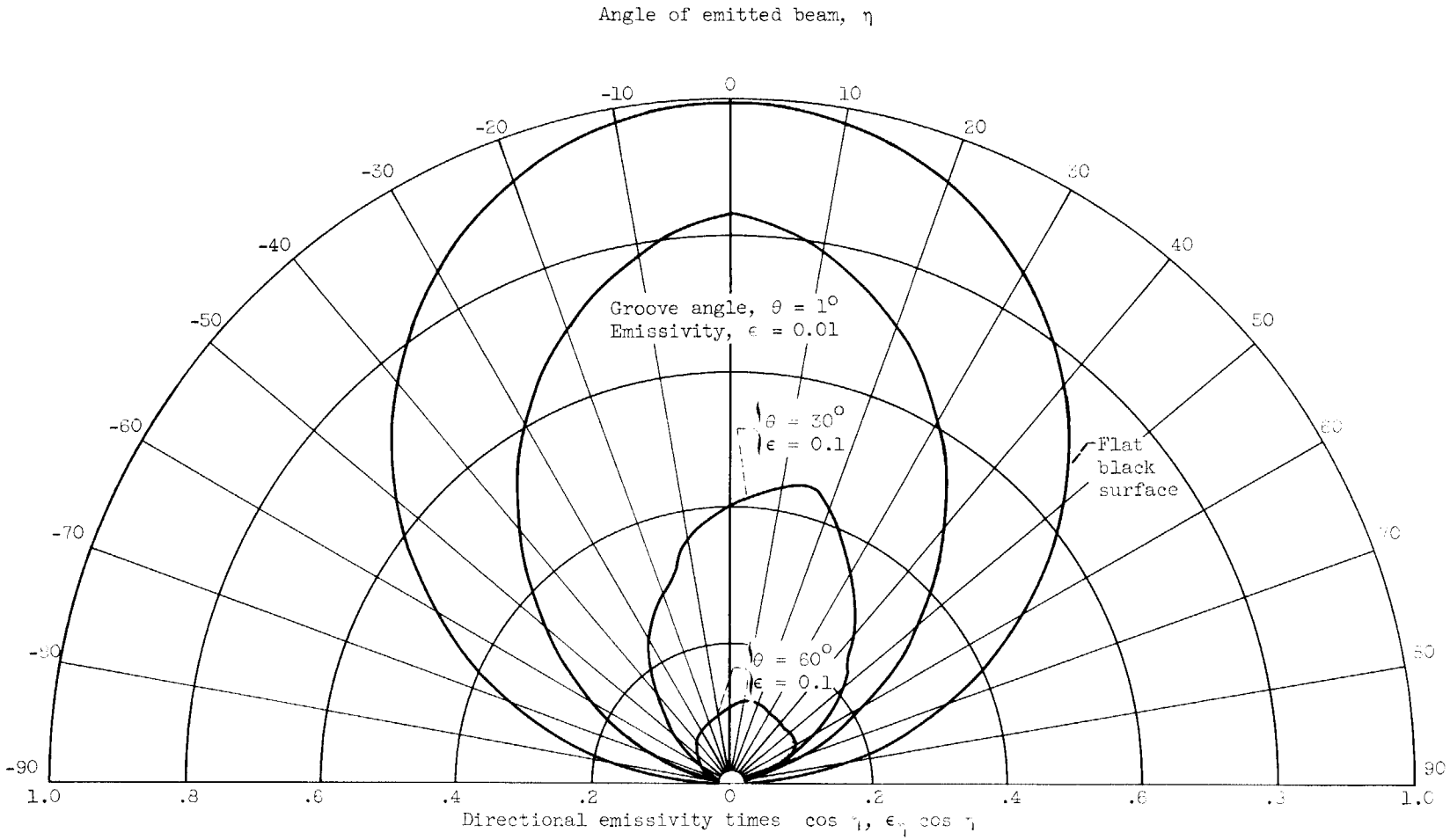

Figure 5. - Distribution of emitted energy.

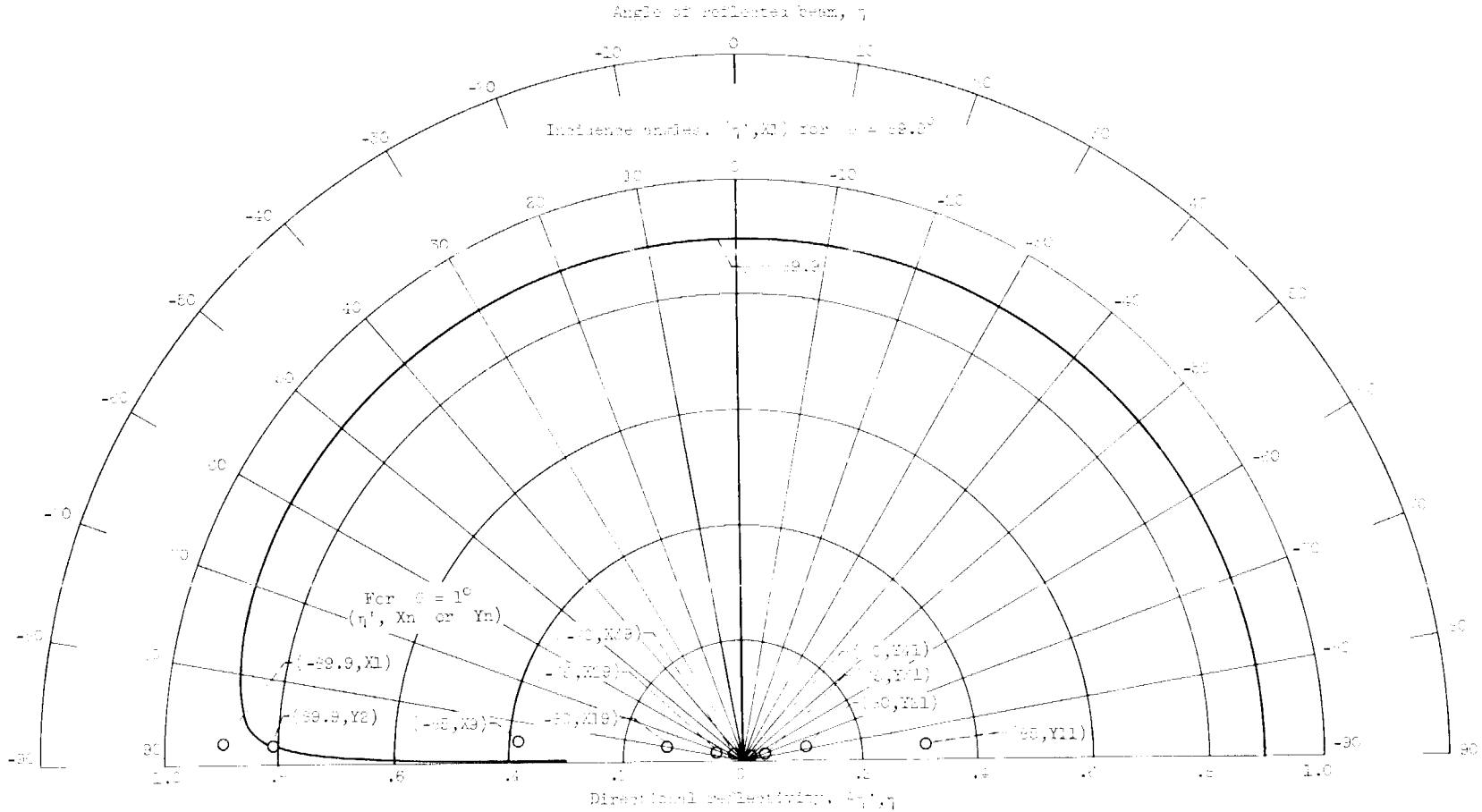

(a) Emissivity of wall, 0.1.

Figure 7. - Directional reflectivity of a process surface.

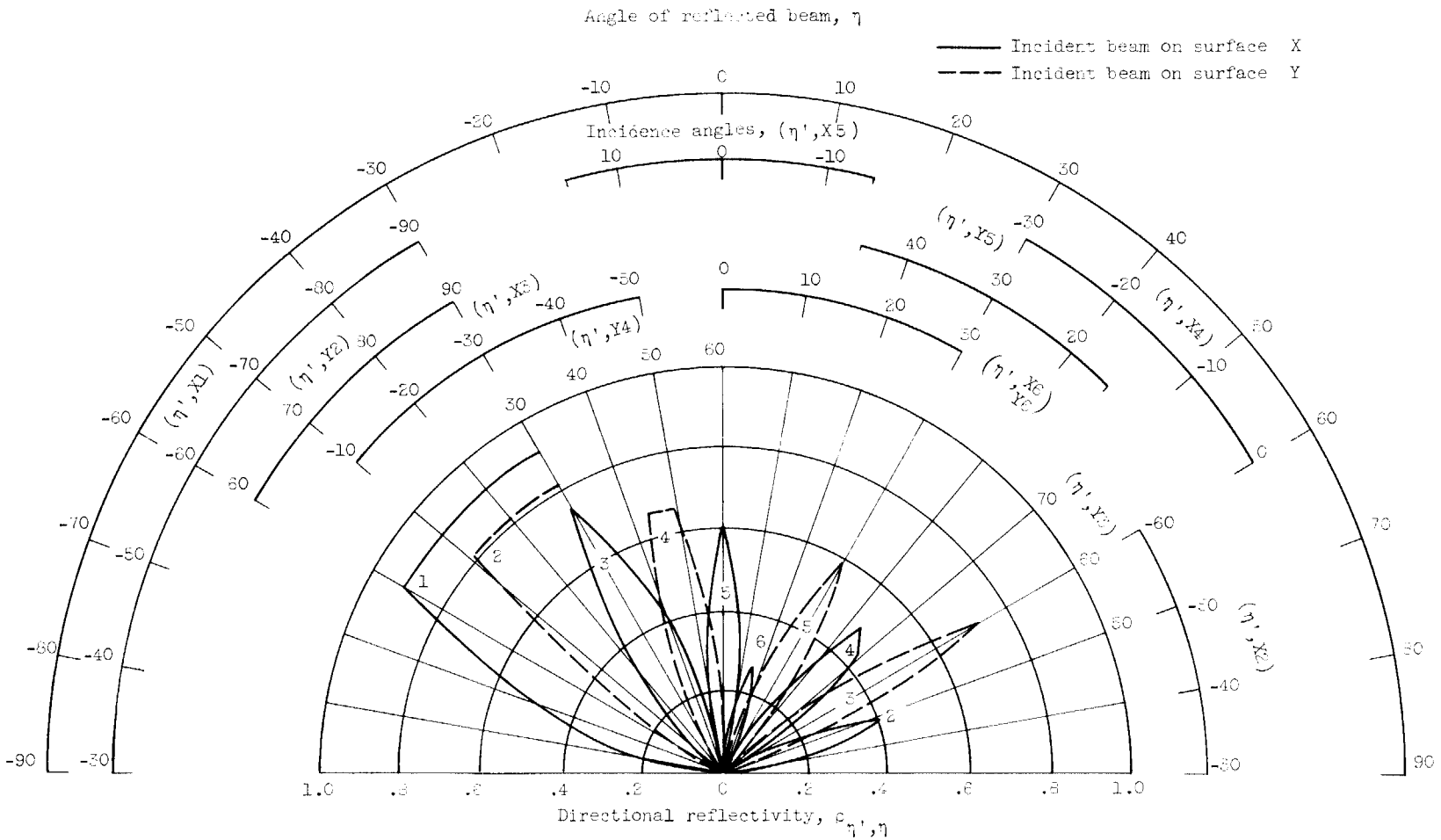

(b) Emissivity of wall, 0.1; open angle between walls of groove, 30°.

Figure 8. - Continued. Directional reflectivity of a grooved surface.

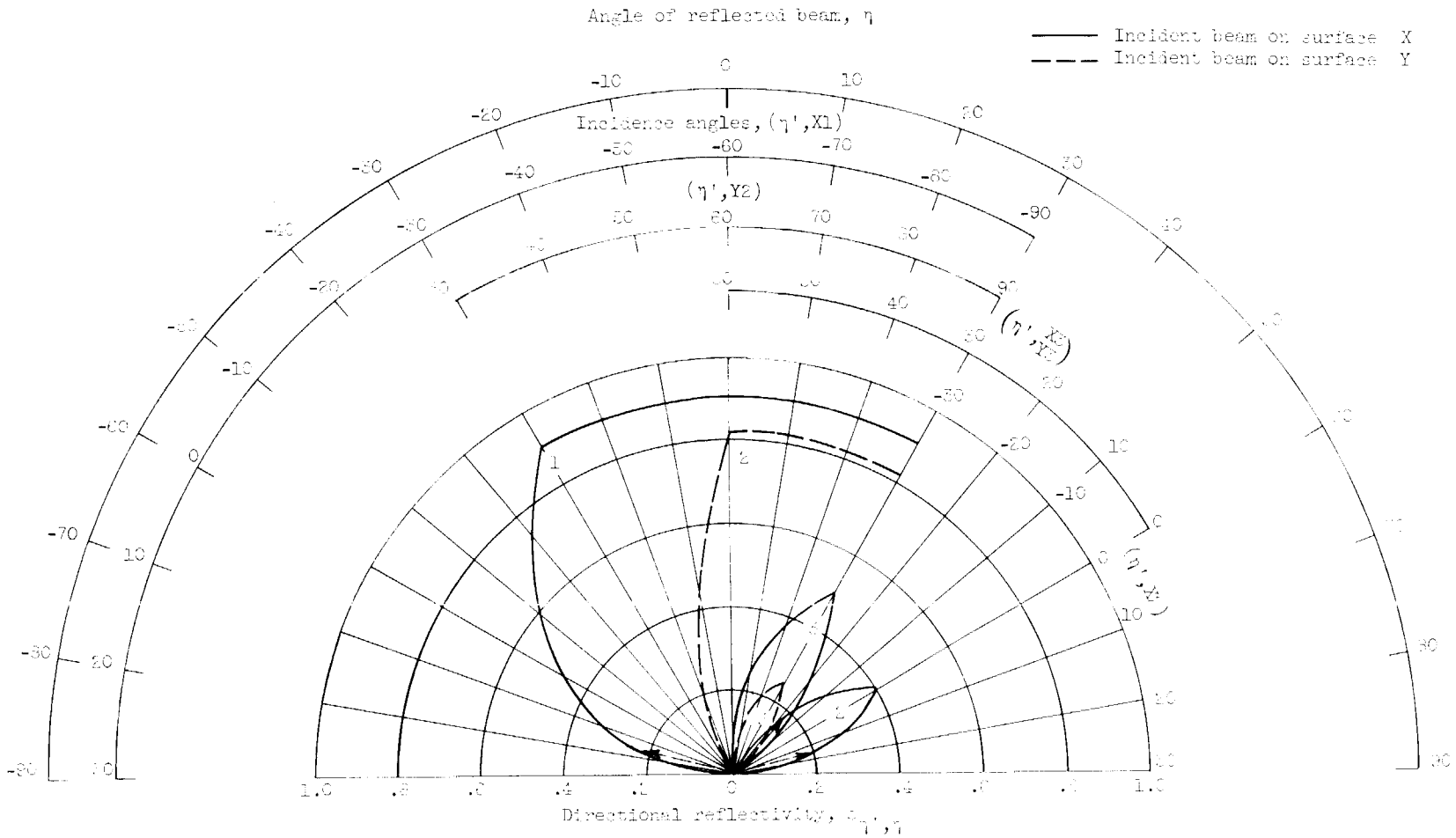

(c) Emissivity of wall, 0.1; open angle between walls of groove, 60°. Arrows refer to reflectivity of incident beam η' = 15°.

Figure 6. - Concluded. Directional reflectivity of a grooved surface.

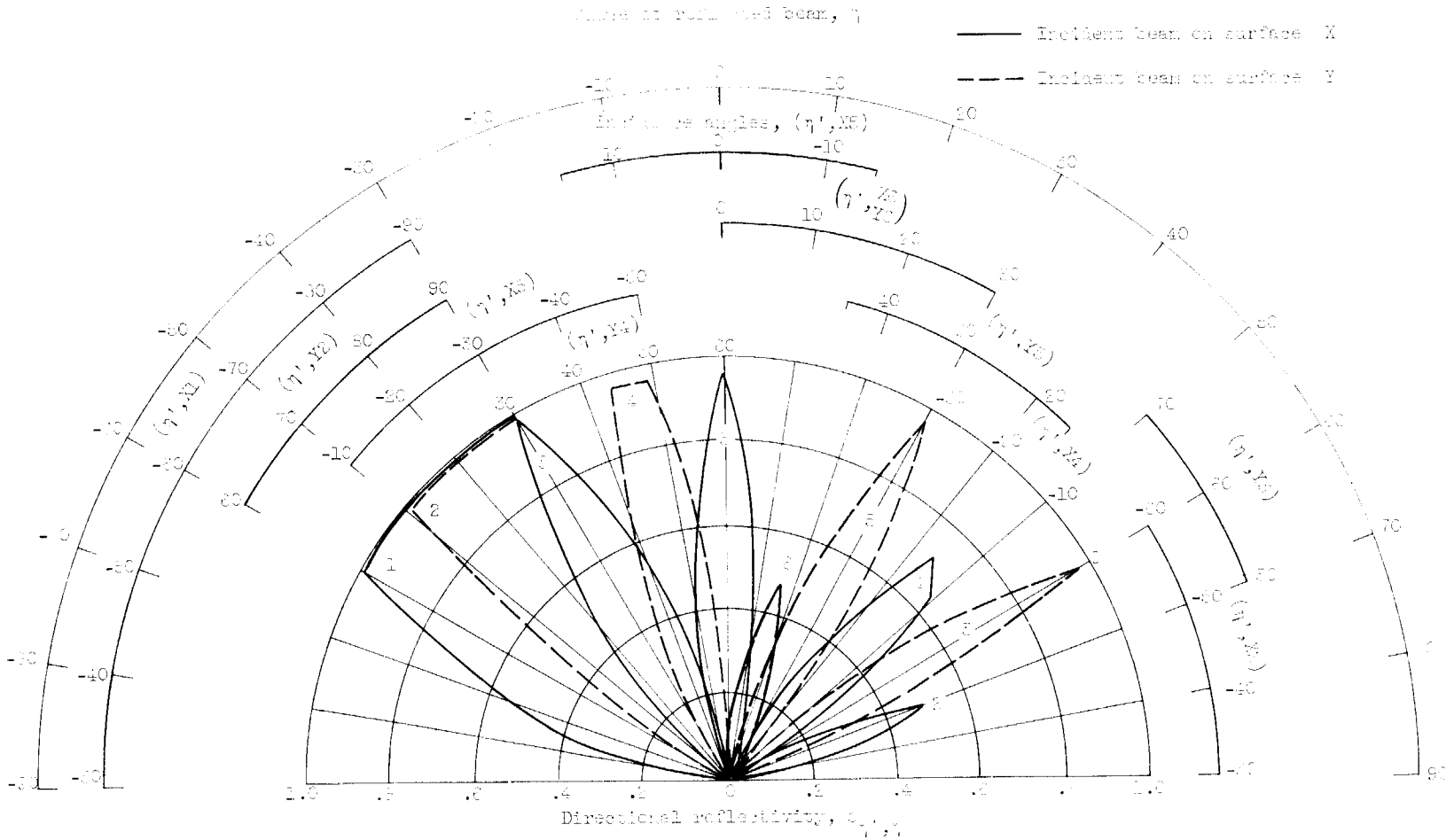

Figure 7. - Directional reflectivity of a grooved surface. Emissivity of wall, 0.11; apex angle between walls of groove, 30°.

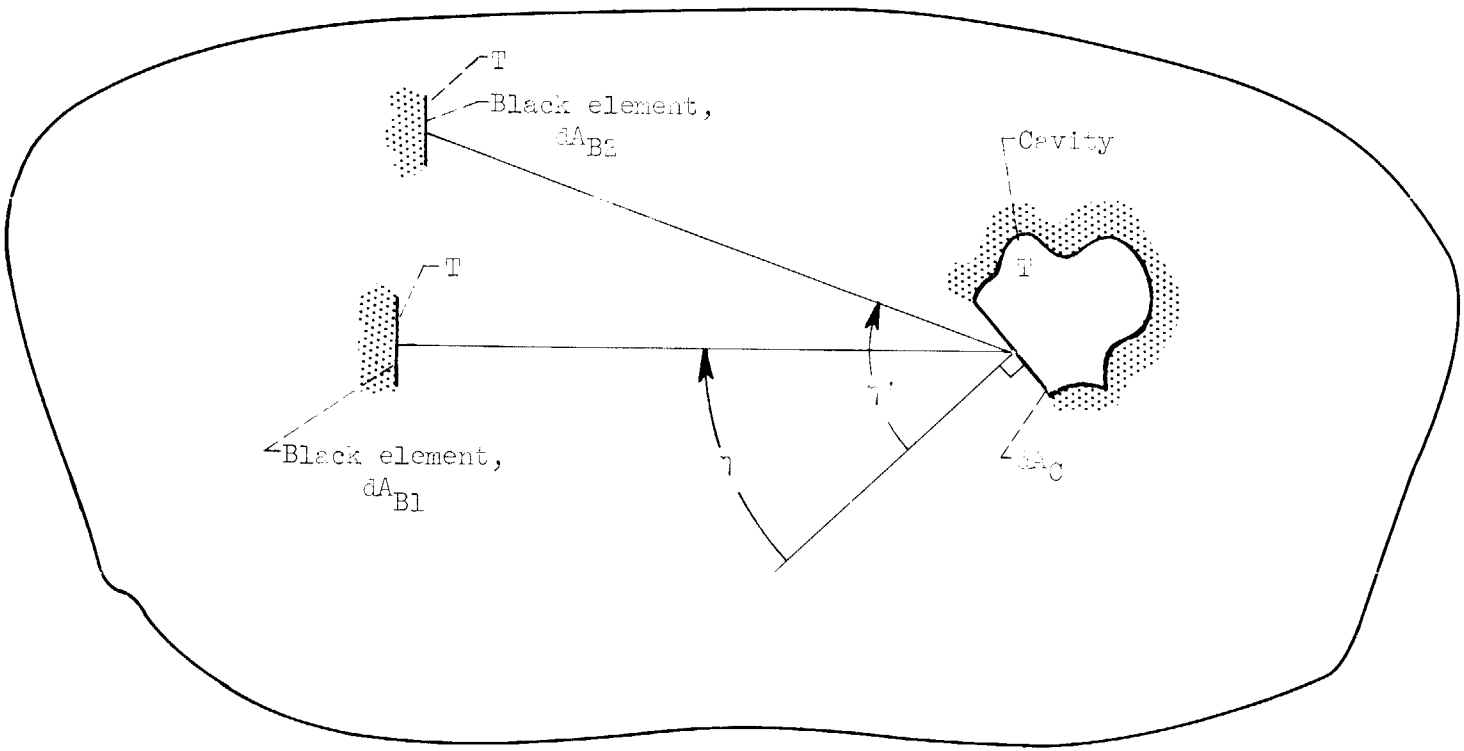

Figure 1. - Isothermal enclosure with flat, black elements and isothermal cavity all at temperature T.

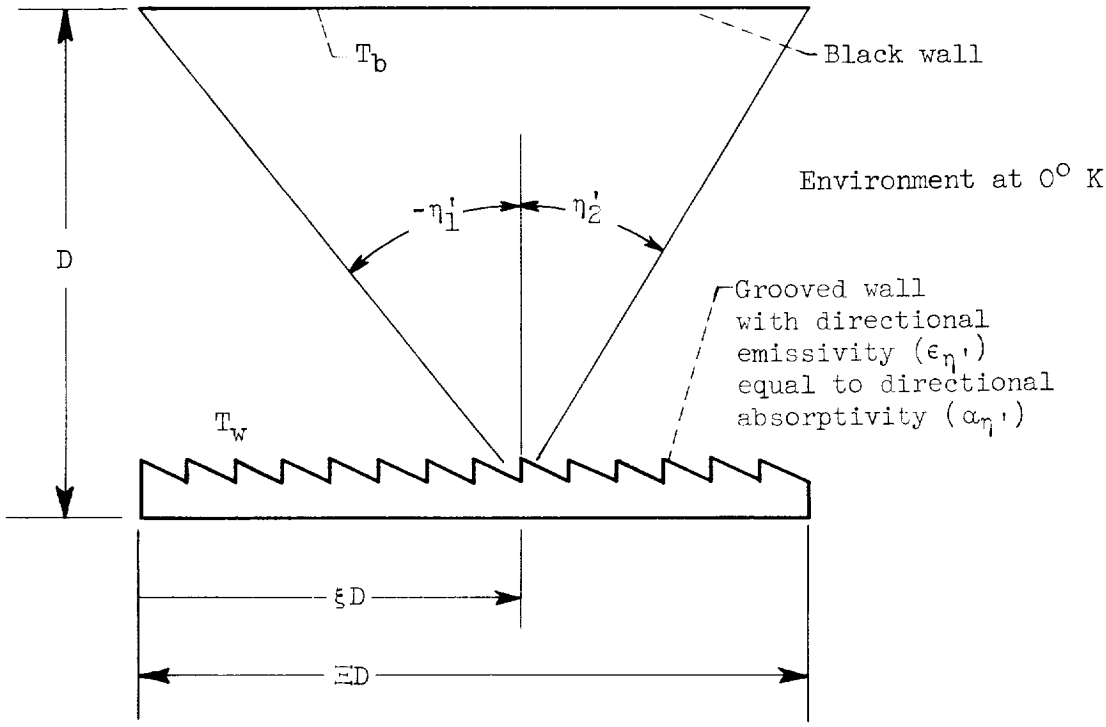

Figure 9. - Radiant interchange between a flat, black wall and a grooved surface.

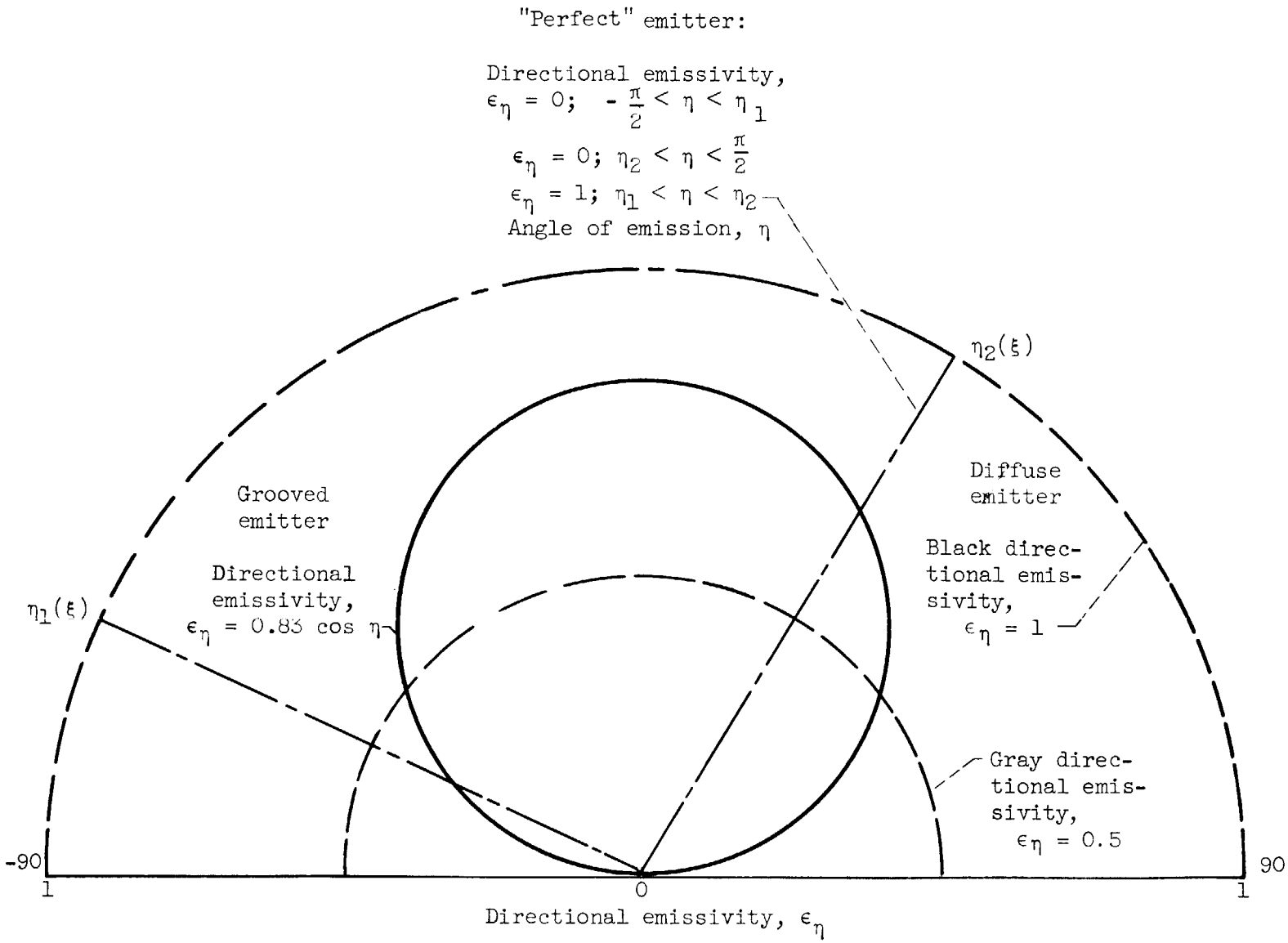

Figure 10. - Directional emissivity at ξ used in examples.

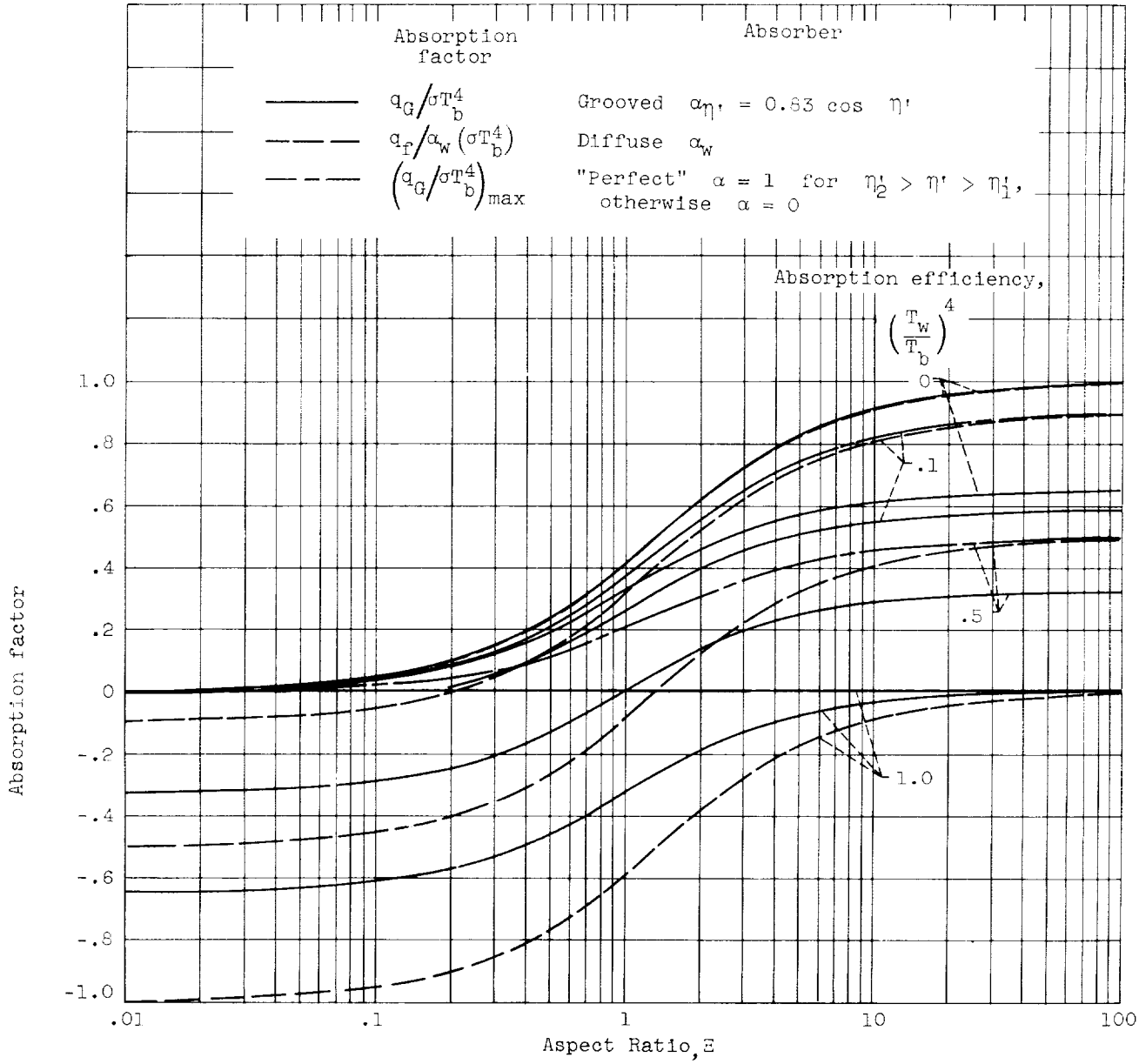

Figure 11. - Absorption factor of various surfaces for different temperature and aspect ratios.

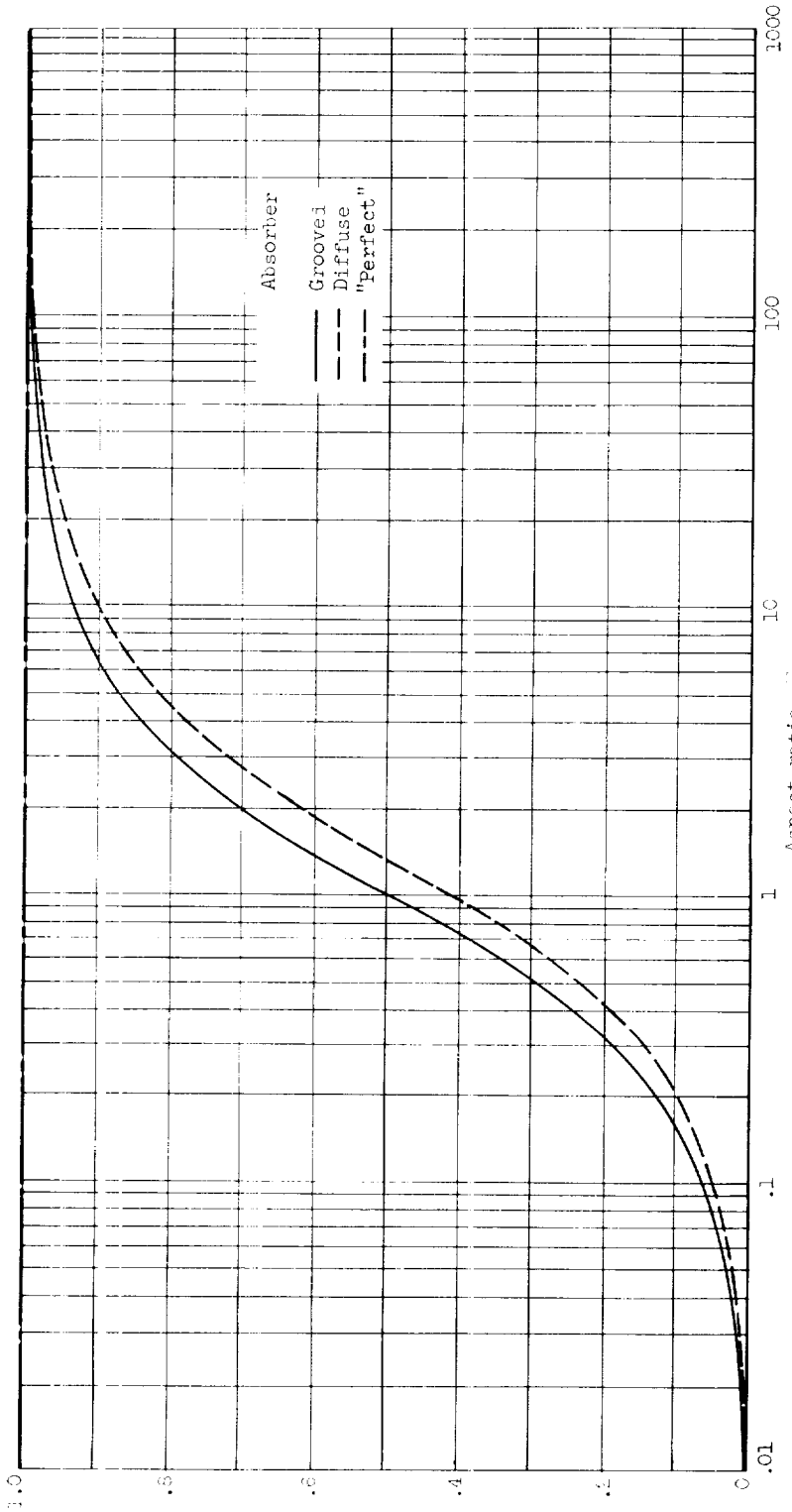

Figure 13. - Absorption efficiency for various absorbing surfaces.

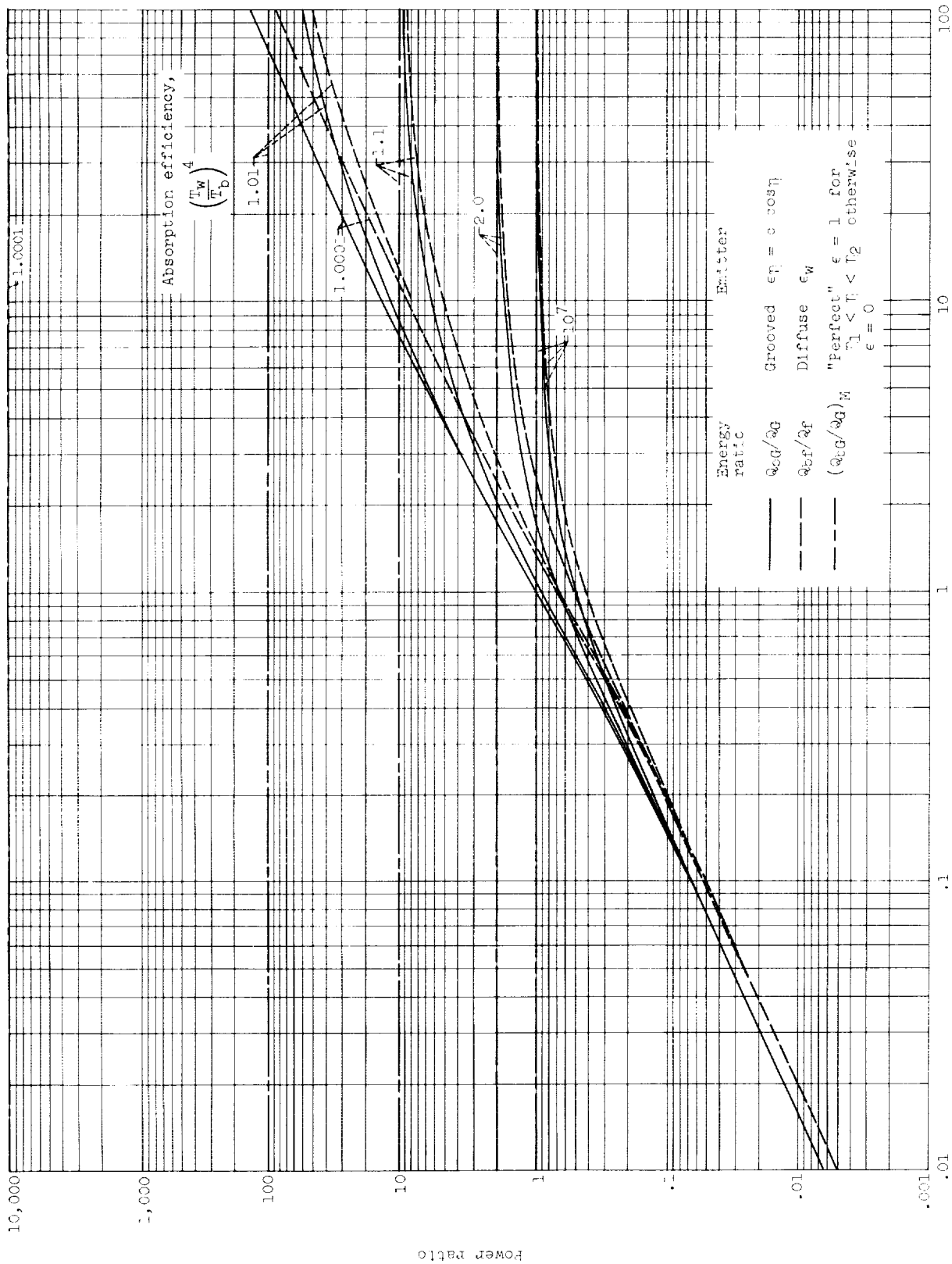

Figure 12. - Ratio of energy incident on black surface to net energy added to emitting surface for different aspect and temperature ratios.